

The Carbon Mineralization Potential of Ultramafic Rocks in British Columbia: A Preliminary Assessment



Dianne Mitchinson, Jamie Cutts, Dominique Fournier, Annika Naylor, Greg Dipple, Craig J. R. Hart, Connor Turvey, Mana Rahimi, and Dejan Milidragovic

Geoscience BC Report 2020-15

MDRU Publication 452



The Carbon Mineralization Potential of Ultramafic Rocks in British Columbia: A Preliminary Assessment

D. Mitchinson¹, J. Cutts², D. Fournier^{1§}, A. Naylor¹, G. Dipple^{1,2}, C.J.R. Hart¹, C. Turvey², M. Rahimi¹, D. Milidragovic^{3†}

Geoscience BC* Report 2020-15

MDRU Publication 452

¹MDRU—Mineral Deposit Research Unit, Department of Earth, Ocean and Atmospheric Sciences, The University of British Columbia, Vancouver, BC, V6T 1Z4 Canada

²BRIMM#—Bradshaw Research Initiative for Minerals and Mining, The University of British Columbia, Vancouver, BC, V6T 1Z4 Canada

³British Columbia Geological Survey, Ministry of Energy, Mines and Petroleum Resources, Victoria, BC, V8W 9N3 Canada

[§]Current Address: Mira Geoscience Ltd., Vancouver, BC, V6C 1T2 Canada

[†]Current Address: Geological Survey of Canada, Natural Resources Canada, 1500-605 Robson St., Vancouver, BC, V6B 5J3 Canada

Keywords: ultramafic, carbon sequestration, serpentinite, British Columbia

Suggested Citation: Mitchinson, D., Cutts, J., Fournier, D., Naylor, A., Dipple, G., Hart, C.J.R., Turvey, C., Rahimi, M., Milidragovic, D. (2020). The Carbon Mineralization Potential of Ultramafic Rocks in British Columbia: A Preliminary Assessment. Geoscience BC Report 2020-15/MDRU Publication 452, 25p.

Report prepared by MDRU[†]

©2020 MDRU—Mineral Deposit Research Unit

Department of Earth, Ocean and Atmospheric Sciences

The University of British Columbia

Vancouver, BC, V6T 1Z4 Canada

Tel: +1-604-822-6136

Email: mdru@eoas.ubc.ca

Includes bibliographic references.

Electronic monograph issued in PDF format.

ISBN 978-0-88865-470-0

*Geoscience BC is an independent, non-profit organization that generates earth science in collaboration with First Nations, local communities, government, academia and the resource sector. Our independent earth science enables informed resource management decisions and attracts investment and jobs. Geoscience BC gratefully acknowledges the financial support of the Province of British Columbia.

[†]MDRU—Mineral Deposit Research Unit is an internationally-recognized collaborative venture between the mining industry and Earth, Ocean and Atmospheric Sciences Department at The University of British Columbia (UBC), established with assistance from the Natural Sciences and Engineering Research Council of Canada (NSERC), and devoted to solving mineral exploration-related problems.

[#]BRIMM, the Bradshaw Research Initiative for Minerals and Mining, connects scientists and engineers across the University of British Columbia (UBC) to promote cross-disciplinary research spanning the entire life-cycle of mining, from early exploration to mine closure and rehabilitation. It operates primarily within the Faculties of Science and Applied Science, connecting several centres of excellence including the Norman B. Keevil Institute for Mining Engineering (NBK), the Mineral Deposit Research Unit (MDRU), and the Hydromet Group. BRIMM supports data integration across the traditional silos of exploration, mining and environmental impact to produce to a greater appreciation of ore diversity for processing and waste management while maximizing the value of information collected at each stage of the mining cycle.

Cover: Field photograph, (Decar Nickel District, B.C.); image of mineralized atmospheric carbon in tailings (Clinton Creek mine, Yukon); and CaMP logo courtesy of MDRU. "Factory Chimney" by Ryuetsu Kato is licensed under the Creative Commons Attribution 3.0 Unported license. Image arrangement by Shannon Guffey.

ABSTRACT

British Columbia contains extensive volumes of ultramafic rock that can sequester carbon dioxide (CO₂) into solid magnesium carbonate minerals to mitigate greenhouse gas (GHG) emissions. Serpentinites, altered hydrated ultramafic rocks, are of particular interest because they can be highly reactive to carbon dioxide at Earth's surface conditions. Serpentinites have distinct magnetic and density properties relative to their unaltered ultramafic protoliths such that they should be identifiable from airborne geophysical surveys. The Carbon Mineralization Potential Project for British Columbia (CaMP-BC) assesses the abundance, location, shape, and areal extent of serpentinized ultramafic rocks in B.C. using existing geological, geochemical, and geophysical data. Preliminary results are reported here. Roughly 46% of the ultramafic rock bodies in B.C. are associated with large magnetic anomalies consistent with extensive serpentinization. The volume of serpentinites in the upper 1 km of the crust in British Columbia is estimated to be 1,000 km³. Sequestration of CO₂ within these rocks will require one of two processes, *ex-situ* carbon mineralization where serpentinite is mined and exposed to CO₂ or *in-situ* carbon mineralization where CO₂ is injected underground. Serpentinite is known to host some of British Columbia's largest nickel deposits and the extraction and crushing of such rocks during mining will unlock their reactivity for *ex-situ* carbon mineralization. The loosely bound and readily leachable magnesium that could be used for *ex-situ* carbon mineralization has an estimated sequestration capacity of 56 Gt CO₂; this represents more than 800 years of GHG emissions in B.C. at current rates. The use of reactive serpentinite tailings from nickel mining as a carbon sink has the potential to make nickel mining carbon neutral or a net carbon sink. Nickel is a critical commodity for decarbonization of the energy and transport sectors. The development of critical metal mines with a high capacity for carbon dioxide mineralization represents an opportunity to decarbonize supply chains for renewable energy and reduce the greenhouse gas footprint of resource development in British Columbia.

1. INTRODUCTION

Most of the carbon on Earth exists in a solid mineral form where it is thermodynamically favoured and stable over geologic time (Kump et al., 2000). It is no surprise, then, that the “holy grail” of carbon sequestration is to convert the carbon dioxide (CO₂) that is present in air and anthropogenic emissions into mineral carbonates (Lackner, 2003), a process referred to as carbon mineralization. This process proceeds naturally during chemical weathering, but at a slow rate. Increased reactive surface area in finely ground ultramafic mine tailings speeds up these reactions (Wilson et al., 2014), thus presenting an opportunity to reduce greenhouse gas (GHG) emissions of some mines. Because the capacity for sequestration in ultramafic tailings is typically much greater than mine emissions, these mines have the potential to become sites of negative emissions, contributing towards permanent carbon removal from the atmosphere.

Ultramafic rocks in British Columbia are derived from two main geological processes: tectonic emplacement of oceanic crust and mantle onto continental margins (e.g., Zagorevski et al., in press), and intrusion of ultramafic mantle-sourced magmas (e.g., Nixon et al., 2015); ultramafic rocks can form from other geological processes but these are less common. In both instances, the ultramafic rocks are formed at depth within the Earth at conditions far from chemical equilibrium with the atmosphere and hydrosphere. They are readily altered when exposed to groundwater and air. Ultramafic rocks can be broadly classified as fresh igneous rocks dominated by olivine and pyroxene, as hydrated versions dominated by serpentine (serpentinites), and as carbonate-altered equivalents that contain talc, magnesite and/or quartz (ophi-carbonate, soapstone, and listwanite). Of these, serpentinites can be highly reactive upon exposure to CO₂ in air. This is because of the accessory phases, such as brucite and hydrotalcite minerals, which form during serpentinization react rapidly with CO₂ (Wilson et al., 2014; Turvey et al., 2018). In the case of mineral deposits hosted in ultramafic rocks, the fine grain-size of the tailings and the increased surface area that result from mineral processing provide a means to accelerate the natural reactions that occur during carbon mineralization carbonation reactions (e.g., Power et al., 2013), thus providing the potential for carbon neutral (or negative) mining operations (e.g., Wilson et al., 2014; Power et al., 2020).

Previous work has focused on inventories of ultramafic rocks to demonstrate the existence of sufficient volumes of ultramafic rocks at or near-surface on the continents to sequester 100s to 1000s of billions of tonnes of CO₂ (Krevor et al., 2009; Kelemen et al., 2011). However, detailed work has shown that the reactivity of these rocks to CO₂ under surface conditions is highly variable and predominantly controlled by mineral content (Vanderzee et al., 2019). The challenge is to identify where the most reactive ultramafic rocks occur and to evaluate scenarios for carbon sequestration by matching CO₂ source-transport-sink adjacencies.

Due to the time-intensive nature of fieldwork and characterization of rocks through reactivity testing (e.g., Seifritz, 1990; Lackner et al., 1997; Thom et al., 2013; Wilson et al., 2014; Lu, 2020) remote-sensing techniques, such as geophysics, can be used to efficiently assess, at a first-order, the reactivity of rocks. Serpentinization and carbonation reactions result in changes in the density and magnetic susceptibility of ultramafic rocks (e.g., Toft et al., 1990; Oufi et al., 2002; Maffione et al., 2014). Pristine, unaltered ophiolitic ultramafic rocks should have densities and magnetic susceptibilities equivalent to those of their constituent primary minerals (3100–3300 kg/m³ and ~1 x 10⁻³ SI, respectively); the latter is directly related to the concentration, distribution, and size of ferro-magnetic minerals, primarily magnetite, which is typically not present as a primary mineral (Tauxe, 2010). Serpentinites are dominated by serpentine ± brucite, which have densities of 2400–2550 kg/m³ (O’Hanley, 1996), and magnetite (e.g., Oufi et al., 2002; Maffione et al., 2014). Serpentinization may cause volume increases of up to 40–50% (e.g., Hostetler et al., 1966) thus, serpentinites are typically less dense and have a higher magnetic susceptibility than their unaltered equivalents (e.g., Toft et al., 1990; Miller and Christensen, 1997; Maffione et al., 2014; Bonnemains et al., 2016). Hydrothermal carbonate alteration can overprint serpentinization and results in the conversion of serpentine, brucite, and magnetite to (hydro-)magnesite, talc, and quartz (Hansen et al., 2005; Kelemen and Matter, 2009; Menzel et al., 2018; Snæbjörnsdóttir et al., 2020); such rocks have densities of 2900–3000 kg/m³. Thus, carbonated ultramafic rocks are denser and have lower magnetic susceptibilities than serpentinites (Hansen et al., 2005).

The goal of the Carbon Mineralization Potential for British Columbia project (CaMP-BC) is to produce an inventory of ultramafic rock localities in B.C. that includes both their mineralization potential (for carbonation) and their abundance. To do this, we are integrating and reinterpreting existing publicly available geologic, geochemical, and geophysical data. Here we present the preliminary findings, including a physical property model for serpentinized ultramafic rocks that is used to constrain geophysical inversions with the goal of assessing the carbon mineralization potential of ultramafic bodies and estimating the volumetric capacity for these rocks for CO₂ sequestration. The geologically well-characterized ultramafic rocks of the Turnagain intrusion in northern B.C. and the Trembleur ophiolitic suite in central B.C. provide case studies to establish a geophysical inversion workflow that will be applied to each prospective ultramafic body in B.C. Based on correlations between the distribution of ultramafic rocks and their magnetic signatures, we present a first-order ranking of ultramafic rock occurrences that will be used to guide decisions on prioritizing sites for current and future modeling. Several of these sites were selected for preliminary 3D volume modeling in this initial stage of work, and we explore the variability in modelled volume estimates as a function of variations in inversion modeling parameters.

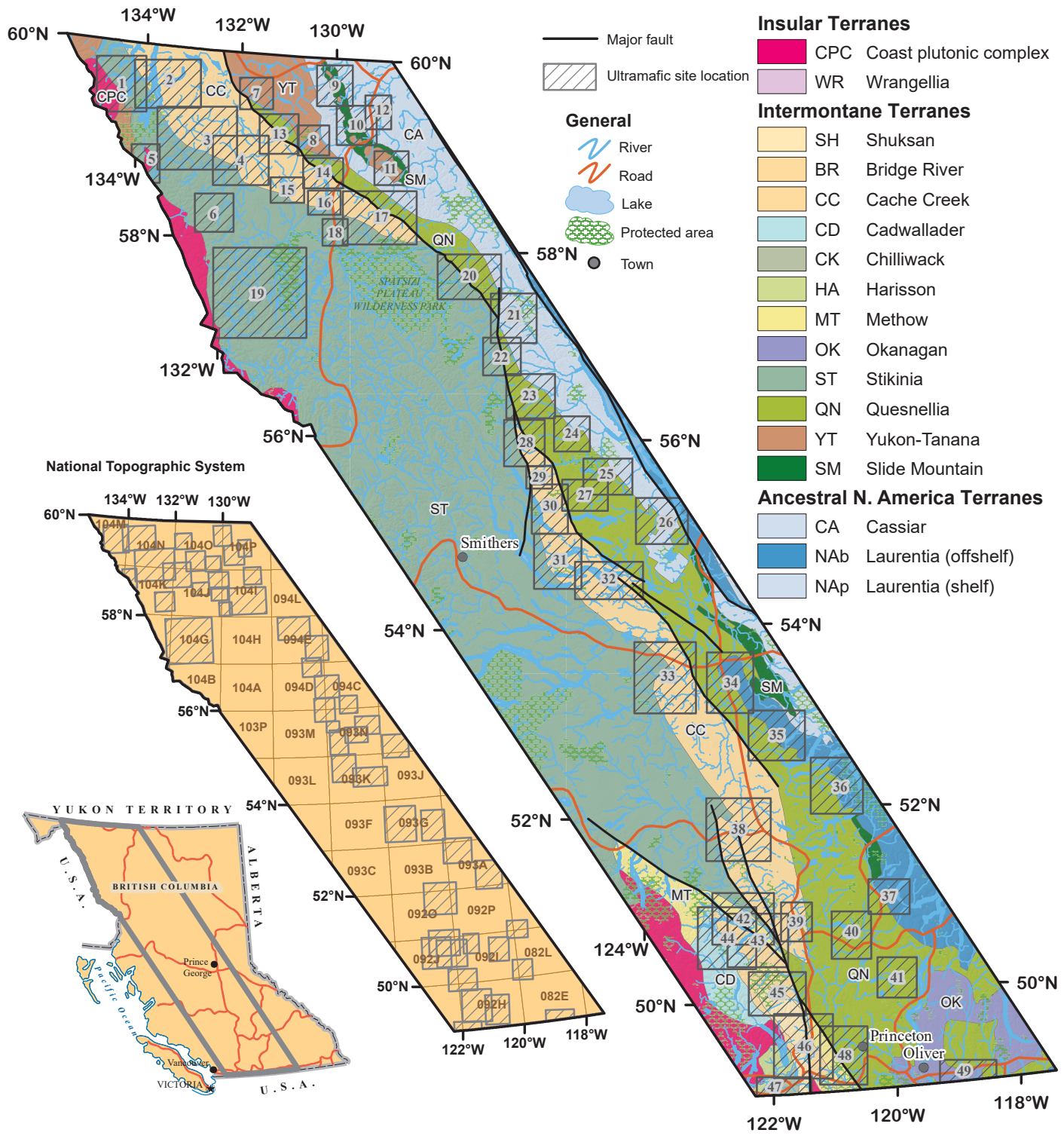
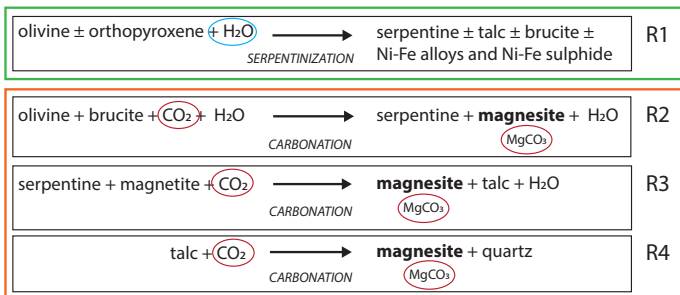


Figure 1: Ultramafic rock localities in British Columbia where carbon mineralization potential was investigated. Noted terranes include Cache Creek (see sections 3 and 6.2), and Atlin, Bridge River, and Slide Mountain (see section 3). The recent subdivision of the northern Cache Creek terrane into the Atlin terrane and Cache Creek complex (Zagorevski et al., *in press*) is not represented.

2. ALTERATION OF ULTRAMAFIC ROCKS

Serpentinization involves the addition of H₂O and hydration of the primary ultramafic minerals. The resulting serpentinite may contain minerals that are highly reactive to CO₂-bearing fluids. The infiltration of CO₂-bearing fluids results in the replacement of hydrous Mg-rich minerals, such as brucite and serpentine, by carbonate minerals, such as (hydro-)magnesite, thereby sequestering atmospheric CO₂.

The general formulae for serpentinization (R1) and carbonation (R2-R4) involve:



3. ULTRAMAFIC ROCKS IN BC

Ultramafic rocks in B.C. occur in two main geologic associations: 1) as basal sections of (dismembered) ophiolites; and 2) as components to Alaskan-type mafic-ultramafic intrusions (e.g., Hancock, 1990; Nixon et al., 2015; 2020; Zagorevski et al., 2017). Ophiolitic ultramafic rocks, which represent accreted slivers of oceanic lithosphere, mainly occur in the Cache Creek (undivided in southern B.C., Atlin terrane in Northern B.C.), Bridge River and Slide Mountain terranes (Fig. 1) (e.g., English et al., 2010; Zagorevski et al., 2017). Intrusive ultramafic rocks are hosted in several arc terranes and were variably emplaced during arc construction, but Alaskan-type intrusions were mostly emplaced during or after accretion of the host-terrane to the ancestral North American margin (e.g., Nixon et al., 2015; 2020). Ultramafic rocks in B.C. have historically been mined for Ni-Cu (e.g., Giant Mascot intrusion: Manor et al., 2016) or have been, and continue to be, targets for advanced mineral exploration projects (e.g., Decar: Britten, 2017; Turnagain intrusion: Nixon et al., 2020).

Forty-nine localities comprising significant ultramafic rock were identified for further evaluation of CO₂ sequestration potential (Fig. 1). These localities were chosen based on geographic groupings of ultramafic bodies that have similar geological and/or geophysical characteristics. To simplify and improve the efficiency of geophysical data analysis, some of the larger 'belts', or clusters of ultramafic rock, were subdivided into several sub-localities, such that no block is larger than 100 km wide.

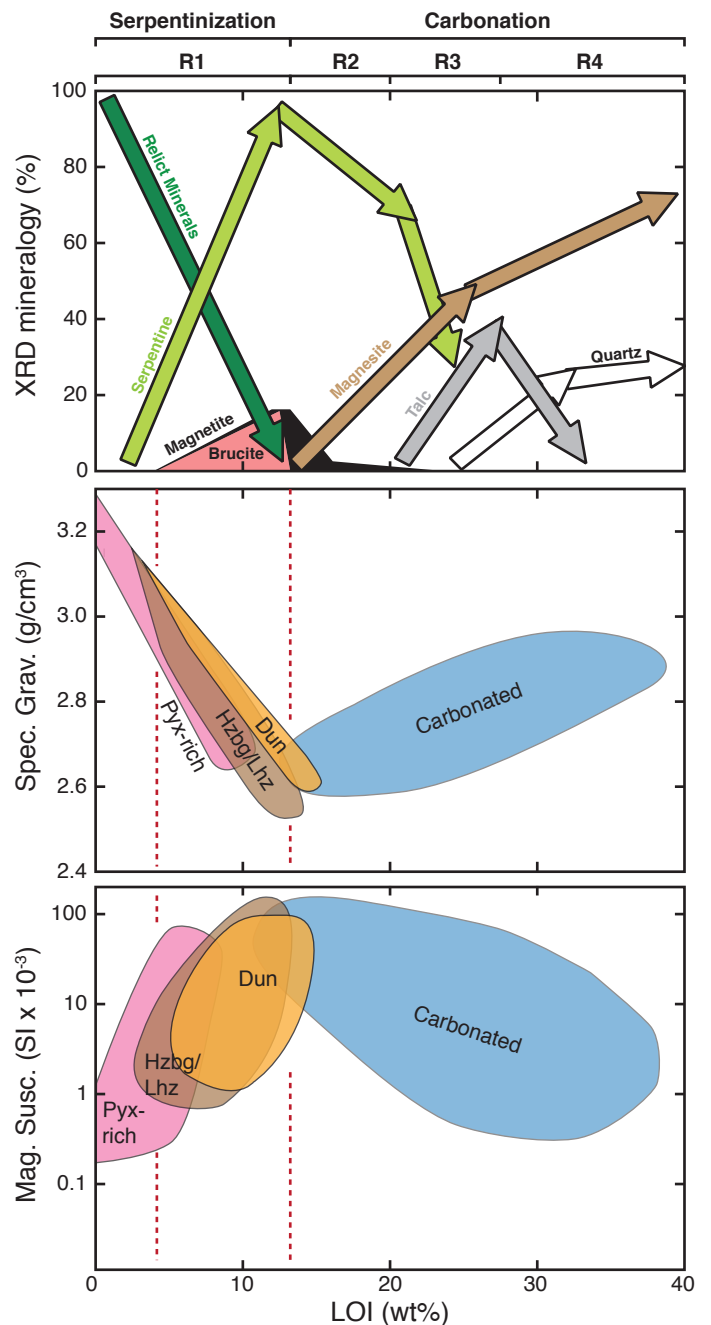


Figure 2: Changes in **a)** mineralogy; **b)** density; and **c)** magnetic susceptibility vs. LOI during serpentinization (R1) and carbonation (R2-R4). During serpentinization (0–14 wt% LOI), abundances of relict primary and serpentine-group minerals decrease and increase, respectively and this is associated with a decrease in density and an increase in magnetic susceptibility. Carbonation sees the destruction of serpentine minerals and formation of magnesite, talc, and quartz, and with these changes in mineralogy, an increase in density and a decrease in magnetic susceptibility.

4. PROPERTIES OF ULTRAMAFIC ROCKS IN B.C.

4.1 Methods

A comprehensive set of rock and core samples from across British Columbia and southernmost Yukon (Table 1) forms the basis for our physical property models (Fig. 2). Physical properties were measured on 402 ophiolitic and 193 intrusive ultramafic rock samples (Table 1) at the Department of Earth, Ocean and Atmospheric Sciences, University of British Columbia (UBC-EOAS). Ophiolitic rocks are the focus of this report, alongside a preliminary dataset for the intrusive samples. A subset of representative ophiolitic samples (n=123) was analyzed at the Paleomagnetism and Petrophysics Laboratory (PPL) at the Geological Survey of Canada-Pacific in Sidney, B.C. to assess the accuracy of magnetic susceptibility and density measurements as well as to provide additional information on the natural remanent magnetization and porosity. The two datasets show a near 1:1 linear correlation, thus, validating the use of our larger internally analyzed dataset. For all instrumentation details for analyses

done at UBC-EOAS and at PPL, see Cutts et al. (2020). Mineral abundance estimates on a subset of samples (Table 1) were determined by quantitative X-ray diffraction at the Electron Microbeam and X-ray Diffraction Facility at UBC-EOAS; these abundances are used to track the mineralogical changes that occurred during serpentinization and carbonation. Full details of all datasets are forthcoming.

4.2 Ultramafic rock physical property model

To assess the variation of physical properties with alteration and lithology, changes in mineralogy and physical properties were compared to loss on ignition (LOI) of the samples. The LOI reflects the total volatile content (primarily H₂O and CO₂) in the rocks and is a geochemical proxy for rock alteration. The generalized physical property-lithology model, as it relates to the degree of serpentinization and carbonation, is shown in Figure 2; the model is strongly controlled by samples from the Atlin and Decar areas (numbered 2 and 31, respectively, in Fig. 1) that comprise 38% and 42% of the UBC-analyzed physical property

Table 1: Location and number of samples used in this study.

UMR Locality (Fig. 1) ¹	Locality (general)	Locality (detail)	Total number of samples (#)	Phys. Prop (UBC) ²	Phys. Prop (GSC) ³	qXRD ⁴
Ophiolitic Rocks						
2	Atlin	City proper	49	43	15	23
2		Monarch Mtn.	137	95	30	119
2		Union Mtn.	5	5	3	0
2		Sentinel Peak	1	1	0	1
2		Mt. Barham	5	5	2	0
2		Marble Dome	3	3	0	1
3	Nahlin	Hardluck Peak	3	3	2	0
3		Menatutuline Range	45	45	17	6
3		Mt. Nimbus	1	1	0	0
3		O'Keefe-Focus	3	3	2	0
3		Nahlin Mtn.	1	1	0	0
3		Peridotite Peak	2	2	2	2
3		Hatin Lake	4	4	0	0
3		Sunday Peak	2	2	0	0
N/A	S. Yukon	Jake's Corner/Squanga Lake	16	16	0	2
31	Decar	Baptiste	62	60	8	33
31		Van	15	15	5	8
31		Mt. S-W	23	23	10	17
31		Other	37	36	13	26
28		Hogem	20	19	4	0
17	King Mtn.	King Mtn.	20	20	10	6
		Sub-Total	454	402	123	244
Intrusive Rocks						
17	Turnagain	DJ/DB	36	36	0	11
17		Horsetrail	53	53	0	9
17		Cliff	4	4	0	1
17		Highland	5	5	0	0
23	Polaris	Polaris	95	95	0	0
		Sub-Total	193	193	0	21
		Total	647	595	123	265

¹ Sample locality referenced to Figure 1

² Number of samples with physical properties measured at UBC-EOAS

³ Number of samples with physical properties measured at GSC

⁴ Number of samples with quantitative X-ray diffraction data

dataset, respectively (Table 1).

Fully serpentinized ultramafic rocks typically have 12–13 wt.% H₂O (Deschamps et al., 2013) and contain very little CO₂ (<1 wt%). Serpentinization consumes primary minerals (olivine, orthopyroxene, and clinopyroxene) and results in a corresponding increase in serpentine-group minerals; in general, the abundances of brucite+magnetite+serpentine add up to ~100% (Fig. 2a). Brucite first appears at ~5 wt% LOI (30–35% serpentinization) and persists in the assemblage until 13 wt% LOI, while magnetite first appears at ~8 wt% LOI, is most abundant from 11–14 wt% LOI, and decreases in abundances thereafter (Fig. 2a). Serpentinization results in a clear, consistent decrease in specific gravity from 3300 to 2600–2500 kg/m³ up to ~14 wt% LOI, although rocks with greater olivine contents tend to have higher LOI at a given density. The decrease in density is proportional to the decrease in relict mineral abundance and mirrors the increase in serpentine (Fig. 2b). Magnetic susceptibility broadly increases during serpentinization from <1 to >100 x 10⁻³ SI; although values show variability up to 2 orders of magnitude at any given LOI. Nevertheless, rocks that are >60% serpentinized (~8 wt% LOI) typically have magnetic susceptibilities of >20 x 10⁻³ SI (Fig. 2c). Carbonation results in a linear increase in density from 2600 to 2900–3000 kg/m³ (Fig. 2b) and this broadly correlates with the increase in magnesite content. Magnetic susceptibility broadly decreases during carbonation (Fig. 2c).

The most highly reactive rocks for carbon sequestration are those containing the highest brucite contents and these typically correspond to rocks that are 60–100% serpentinized (8–13 wt% LOI). For ophiolitic ultramafic rocks, this interval corresponds to densities of 2500–2900 kg/cm³ and magnetic susceptibilities that are typically 20–150 x 10⁻³ SI; the 1st and 3rd quartile values (Q1 and Q3) for samples that are >60% serpentinized correspond to 20 and 75 x 10⁻³ SI, respectively (Fig. 3). These magnetic susceptibility values are of particular interest as we can use them to analyze magnetic data to determine the location and distribution of serpentinized ultramafic rocks. There is an excellent spatial coverage of relatively high-resolution magnetic surveys in B.C. that allow for a province-wide assessment of the magnetic signatures of ultramafic rocks. Unfortunately, gravity surveys at a similar resolution are rare, thus correlation between magnetic and gravity responses indicative of serpentinized rock are not possible at province scale. For intrusive ultramafic rocks, the quantitative mineralogy-physical property model is in progress. However, preliminary physical property data suggest that the median magnetic susceptibility values for olivine-bearing reactive lithologies (dunite-wehrlite-olivine clinopyroxenite) are slightly lower than those of ophiolitic rocks; this is not particularly surprising since intrusive ultramafic rocks in B.C. are commonly less serpentinized than ophiolitic rocks. Despite the slightly lower mean magnetic susceptibility for olivine-bearing intrusive rocks, their Q1 and Q3 are similar to ophiolitic rocks although, notably, there are more outlier intrusive samples with high (>100 x 10⁻³ SI) values (Fig. 3). For this preliminary report

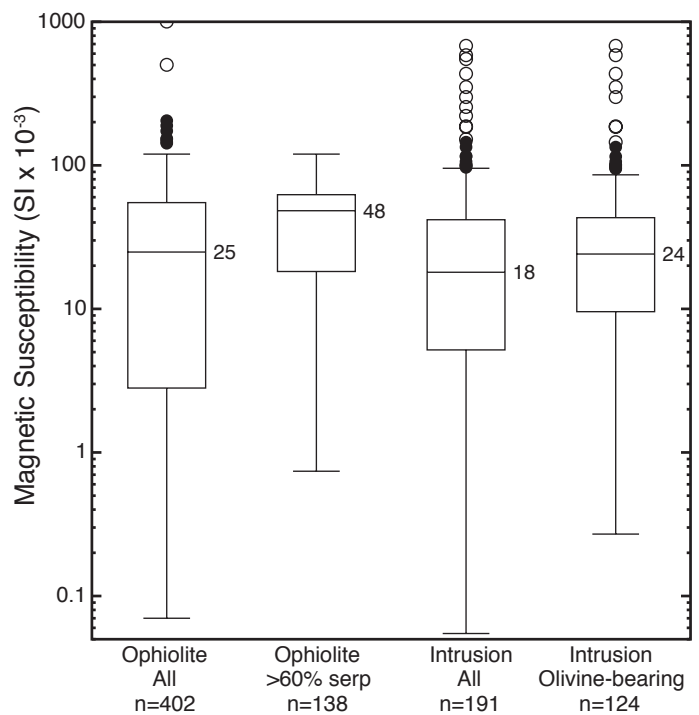


Figure 3: Box-and-whisker plots comparing the distribution of magnetic susceptibilities for all ophiolitic samples, reactive (>60% serpentinized) ophiolitic samples with >8 wt% LOI, all intrusion samples, and olivine-bearing intrusion samples. The horizontal line within each box represents the median with the box drawn around the interquartile range (IQR). Outliers were identified based on the Tukey outlier selection test where the filled circles represent values that are >1.5 x IQR and open circles represent values that are >3 x IQR.

we use the Q1 value as the lower threshold for the magnetic volumes included in our inversions and we consider the Q3 value as representing the typical upper threshold for highly-serpentinized rocks that are used in all synthetic models.

5. PRELIMINARY ASSESSMENT OF PROSPECTIVE ULTRAMAFIC ROCKS IN BC BASED ON MAGNETICS

The ultramafic rock physical property model established above provides the basis for a preliminary 2D assessment of serpentinized ultramafic rock from available magnetic datasets covering B.C. The expectation is that uncarbonated serpentinites are associated with high magnetic susceptibilities, and thus yield positive magnetic responses.

Two datasets are used for an initial 2D assessment of the area of serpentinized rocks in B.C.: the bedrock geology map of British Columbia (Cui et al., 2017), and the Natural Resources Canada (NRCAN) 200 m gridded magnetic data (Natural Resources Canada, 2020). Each polygon, identified as an ultramafic occurrence within the B.C. bedrock geology database, was visually compared against the NRCAN magnetic data to determine whether it coincides with a positive magnetic anomaly, which could suggest the presence of magnetite-bearing serpentinized rock. Approximately 750 polygons were assessed and assigned one of eight

Table 2: Classification system for ultramafic rock polygons from the BCGS bedrock geology database.

Classification	Description	Confidence that magnetic anomaly is related to mapped ultramafic unit	Number of polygons represented	Total Area (km ²) of mapped polygons within class
A	Positive magnetic anomaly well-correlated spatially to mapped ultramafic polygon	High	78	1681
B	Positive magnetic anomaly extends beyond mapped ultramafic polygon	High	105	232
C	Irregular or patchy positive magnetic anomaly contained within a mapped ultramafic polygon	High	158	958
D	Polygon with offset positive magnetic anomaly (may be due to the ultramafic or adjacent unit)	Low	39	119
E	Can't isolate/differentiate a distinct magnetic signal from surrounding magnetic material	Low	38	39
F	Very weak to no magnetic signal correlated to the mapped ultramafic polygon	None	95	733
X	Generally small polygon of varied magnetic response, overall insignificant contribution to ultramafic rock volume	None	210	56
ND	No magnetic data coverage	None	23	9
Total			746	3827

designations: A, B, C, D, E, F, X, and ND (Table 2). Figure 4a provides an example from the Atlin area demonstrating how classifications were assigned:

Classification A is assigned to polygons that show a very similar spatial correlation with a magnetic high and, as such, the area and volumes derived for this class have a high confidence ranking

Classification B is assigned where the magnetic anomaly extends beyond the mapped polygon, and thus, an area and volume based on the polygon is expected to be underestimated

Classification C is assigned where the magnetic response is 'patchy' or domainal within the polygon; magnetic domains are expected to represent serpentinized rock, while magnetic lows may be unaltered ultramafic rocks, zones of carbonate alteration, or intercalation of other rock types.

Classifications D and E describe polygons where there is a magnetic response but due to other magnetic sources nearby, the response cannot confidently be attributed to the ultramafic rock.

Classification F is a polygon with a very weak, or no positive magnetic signal.

Classification X corresponds generally to a very small or insignificant polygon relative to the scale of the investigation.

ND means no NRCan magnetic data is available.

From the initial assessment of the total area of magnetic signatures of ultramafic rocks in B.C. it is possible to estimate a preliminary volume of magnetic serpentinized ultramafic material (Table 2). A total of 341 of the 746 polygons underlain by ultramafic rock are captured within groups A, B, or C, representing 46 % of all ultramafic polygons in the BCGS bedrock geology database (see province-wide distribution of classified polygons in Figure 5). The 341 polygons represent an aerial extent of 2,871 km² or 75 % of the total ultramafic polygon area of 3,827 km². Assuming an average depth of 1 km, which is a reasonable though arbitrary expectation of mining depth consistent with the imbricated and thin thrust slices of many surface exposures of ophiolitic ultramafic occurrences in B.C., this equates to a potential carbon mineralization volume of 2,871 km³. This calculation represents a simple estimation of serpentinized rock volume in B.C. based solely on mapped or interpreted ultramafic occurrences that are recognized as correlating with magnetic highs. The relationships between the extents of the mapped units and magnetic responses is not typically perfectly coincident, and the distribution of serpentinization within an ultramafic unit is likely to be variable. It is expected that more geologically realistic volumes can be calculated through 3D geophysical inversion of individual magnetic anomalies.

6. SITE-SPECIFIC CASE STUDIES TO INFORM GEOPHYSICAL INVERSIONS

Two ultramafic localities in B.C. were chosen for detailed analysis to calibrate and validate detailed geophysical interpretation: the Turnagain Alaskan-type ultramafic intrusion and the Decar Nickel district within the Trembleur Ophiolite. Both areas bene-

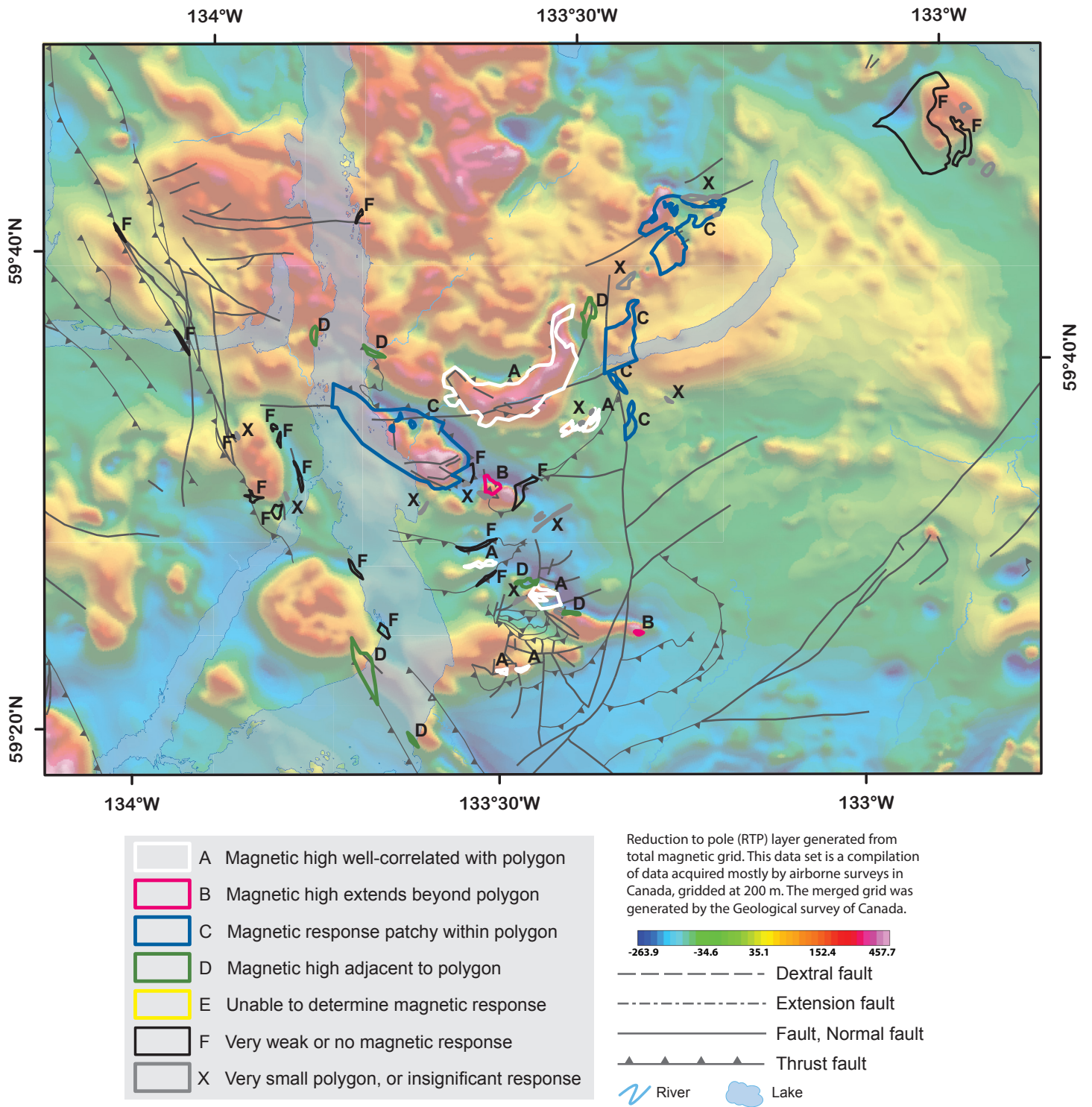


Figure 4: Example of the classes assigned to the B.C. Geological Survey (BCGS) bedrock geology ultramafic polygons based on their spatial relationship to magnetic anomalies; area shown is ultramafic locality 2 in Figure 1.

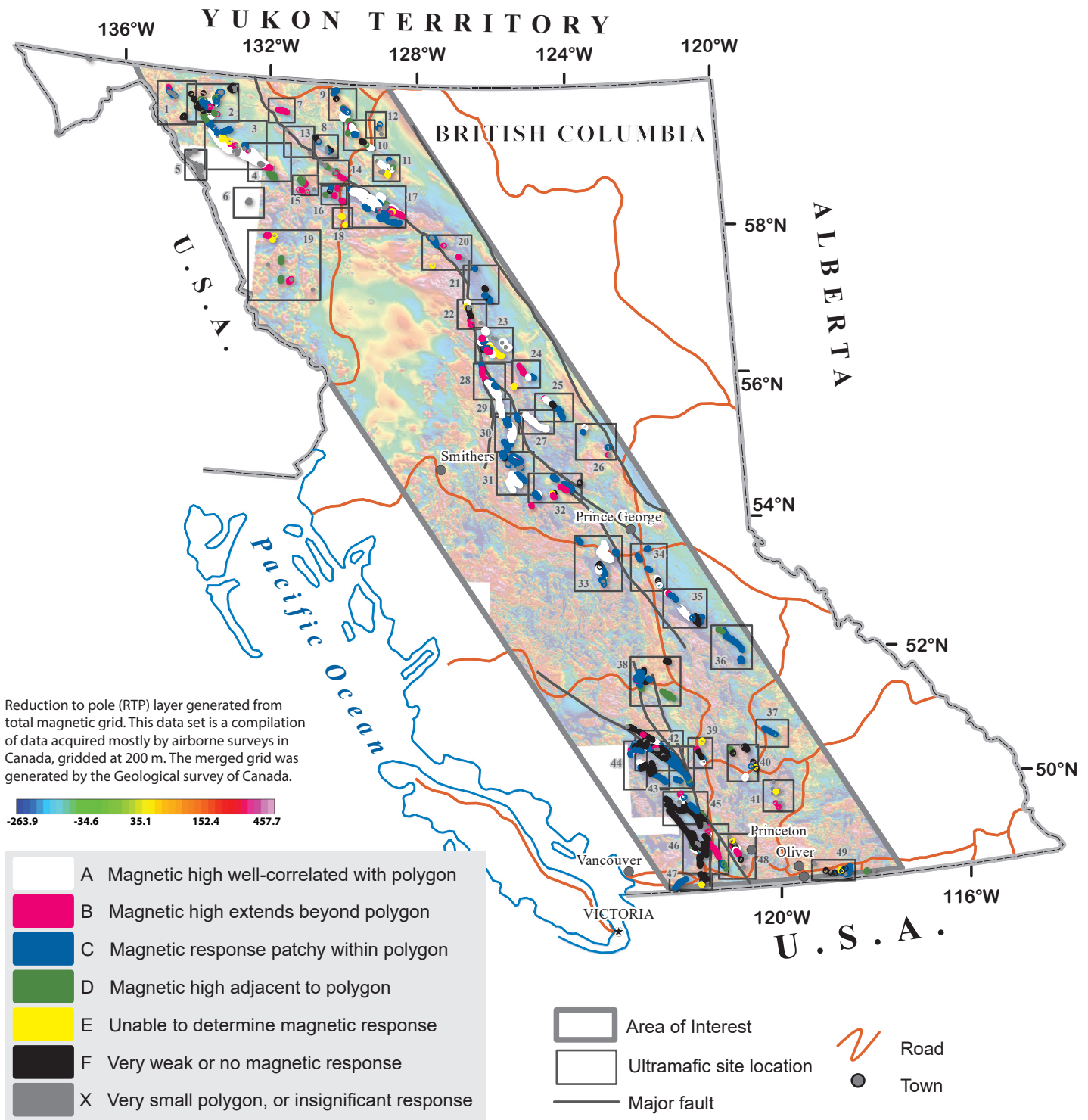


Figure 5: Province-wide distribution of mapped and interpreted ultramafic units from the B.C. bedrock geology database colored according to a classification assigned based on spatial relationship between each polygon and positive magnetic anomalies.

fit from detailed geological characterization, and high-resolution geophysical data. The Turnagain ultramafic intrusion (Nixon et al., 2017; 2020) was chosen as a case study site for comparison of the outcomes of inversions using lower versus higher-resolution data. Turnagain has been the focus of significant historical exploration for Ni mineralization and hosts a significant resource in the Turnagain Nickel deposit (Mudd and Jowitt, 2014). Detailed geological mapping and exploration geophysical survey data are available at this locality (Jackson-Brown et al., 2014; Nixon et al., 2017; 2020). The Decar Nickel District was selected as a case study site to further test volume estimation from magnetic inversion, and to explore the effect of remanence on inversion results. The site benefits from having extensive drilling, recent mapping (Milidragovic, 2019), detailed lithological/geochemical data (e.g., Britten, 2017; Milidragovic et al., 2018; Milidragovic and Grundy, 2019; Steinhorsdottir et al., 2020), and detailed aeromagnetic survey coverage.

6.1 Turnagain site investigation of recovered volumes from low- and high-resolution magnetic data

The Turnagain Alaskan-type ultramafic intrusion (Fig. 6) is approximately 25 km² in size and is located 70 km east of the community of Dease Lake in north-central B.C. The intrusion is Early Jurassic in age and is characterized by an olivine-rich core comprising dunite and wehrlite and olivine-poor marginal regions comprising clinopyroxenite and hornblendite (Nixon et al., 2017; 2020). Contained Ni (and Co) is primarily hosted in dunite, wehrlite, and clinopyroxenite of the Horsetrail zone (Nixon et al., 2017; 2020). Additional Cu-Pt-Pd mineralization is hosted in clinopyroxenite and hornblendite of the DJ-DB zone (Jackson-Brown et al., 2014). The rocks of the Turnagain intrusion have a wide range of magnetic susceptibility values (<0.1–800 x 10⁻³ SI). Olivine-bearing lithologies typically have values of 10–45 x 10⁻³ SI (Q1 and Q3, respectively; Fig. 3) with a relatively large number of outliers at >100 x 10⁻³ SI.

The Turnagain site is covered by both the regional NRCAN magnetic data that are gridded at 200 m (Natural Resources Canada, 2020), and by a higher resolution, 100 m line-spacing aeromagnetic survey completed by Aeroquest in 2004, making it a useful location for comparing results from inversion of lower and higher resolution magnetic data. The ultramafic intrusion is associated with a large magnetic high which, in the high-resolution aeromagnetic data, appears to closely follow the edges of the intrusion (Fig. 7a).

Inversion of the NRCAN residual total field (RTF) magnetic data was done with a Magnetic Vector Inversion (MVI) code made available by the SimPEG open-source package (Cockett et al., 2015). 3D geophysical inversions are typically applied as a method to model the Earth's subsurface, where physical property models of the Earth are calculated from observed geophysical datasets. The MVI approach (Lelievre and Oldenburg, 2009)

recovers the orientation and magnitude of magnetization in 3D without making assumptions about the type of magnetization (e.g. induced or remanent). MVI uses an effective magnetic susceptibility (K_e) to report the strength of magnetization, which combines both the induced and remanent components of magnetization.

As for any geophysical inverse problem, the solution is non-unique, and there are many models that can produce the observed magnetic data. The usual strategy to address this non-uniqueness is to impose constraints such that the recovered magnetizations remain small and smoothly varying in 3D. The assumption is therefore made that physical properties are continuous and slowly varying. This is one possible outcome. In order to further assess variability in possible models that can explain the data, we performed additional inversions with variable constraints (ℓ_p norms) applied to the model values and their spatial gradients (Fournier and Oldenburg, 2020). The choice of ℓ_p norms determines the ultimate blockiness or smoothness and volume of the calculated 3D physical property model. Variable combinations of norms guide the result from a smoothly varying model toward progressively more compact bodies with sharp edges. The choice of ℓ_p norm will have an effect on both the range of effective susceptibility values recovered, and their distribution in space. Generally speaking, ℓ_p norms for $p=2$ (industry standard norm) produce smooth and large anomalies with low model values, while lower norms ($p < 2$) produce a more 'compact' model with higher model values. All these solutions can equally explain the observed magnetic data, but the character of the solution can change based on different geological assumptions. Varying the ℓ_p norm and reviewing the recovered volumes and susceptibilities to determine if they are geologically realistic will inform how future inversions are approached and how volumes of serpentinized material will be estimated.

The effective susceptibility models resulting from the inversion of NRCAN data over Turnagain were thresholded at a lower bound of 20 x 10⁻³ SI to visualize domains of effective susceptibility with values typical of serpentinized ultramafic rocks (Section 4.2). Volume calculations are modelled using this threshold value and a starting point, or 'seed'. Neighbouring model cells in all six directions of the seed are queried and determined to be either above or below the threshold. The process is then expanded outward in all six directions, concluding once cells no longer meet the query. All cells with values confirmed to be above the threshold value were then added to the volume for the given ℓ_p norm model. A rounded body was resolved with volumes ranging from 17–52 km³ (Fig. 7). The top of the high susceptibility zone (>20 x 10⁻³ SI) lies approximately 1000 m below the topographic surface (Fig. 7c). Recovered ranges of effective magnetic susceptibility for L2-L2 and L0-L2 norms are within the expected range of values measured on samples. L0-L1 norms produce models with higher magnetic susceptibilities than other inversions, but still less than 150 x 10⁻³ SI (Fig. 7b).

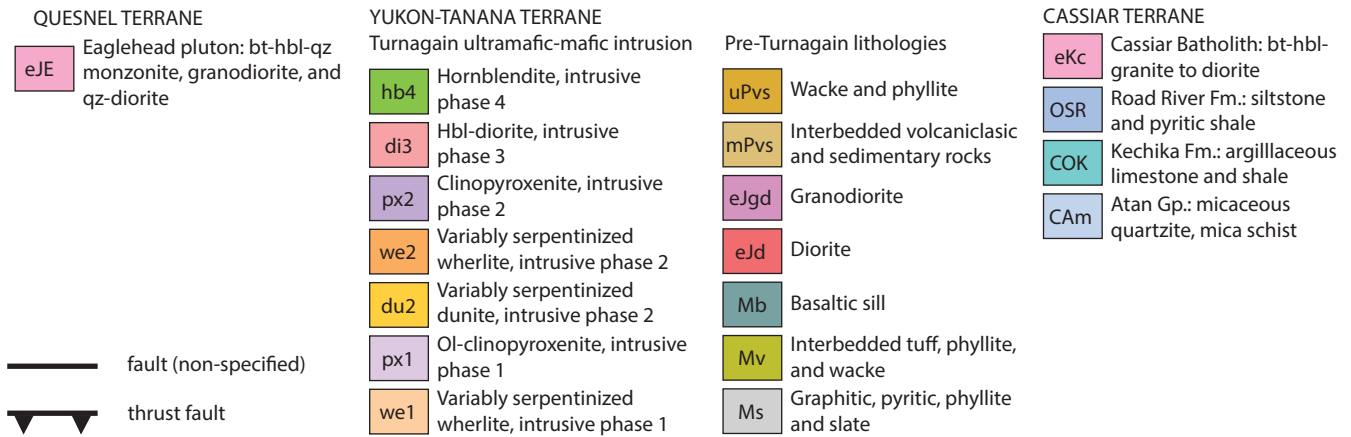
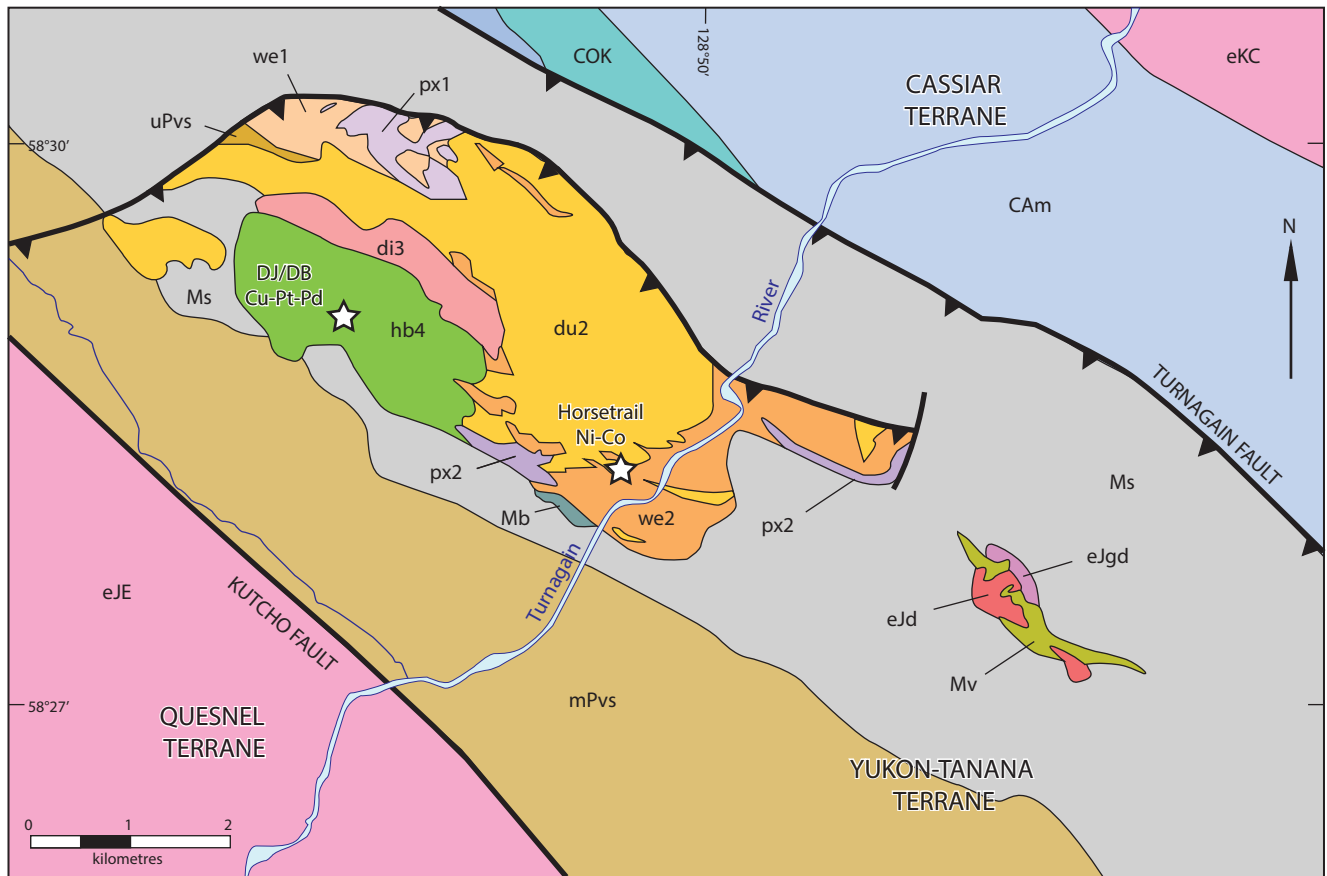


Figure 6: Geological map of the Turnagain ultramafic intrusion (Nixon et al., 2017); this ultramafic locality 17 is shown in Figure 1.

The inversion of Aeroquest high-resolution data reveals a more horseshoe shaped body with high effective susceptibility ($>20 \times 10^{-3}$ SI) zones having volumes of 28–80 km³, depending on the ℓ_p norm applied (Fig. 7d–f). Clearly the higher resolution Aeroquest data yielded a more detailed model result but, notably, in both models, the recovered volumes using the same threshold are similar. The volume of the high effective susceptibility domain derived from the inversion of regional and high resolution magnetic data are similar in median value (40 km³), but the regional data generally retrieve volumes that are 60–65% smaller than those from the high resolution data.

In both models, the base of the serpentinized rocks occurs at around 1500 m below sea level; however, unlike the NRCAN mag-

netic data inversion result, the higher resolution data inversion recovers high effective susceptibility material near-surface. The deeper-seated core of the high effective susceptibility volume from the NRCAN data inversion (Fig. 7c) is not considered realistic considering that high susceptibility ultramafic rocks were collected at the surface at the Turnagain site, and are expected to occur to depths of only around 1000 m. The volume consistency between the two inversions is encouraging, but the deeper placement of mass using the NRCAN data is not consistent with the known geology. In future work, efforts will be invested to reconcile the two datasets through susceptibility bound values, model depth weightings and data levelling.

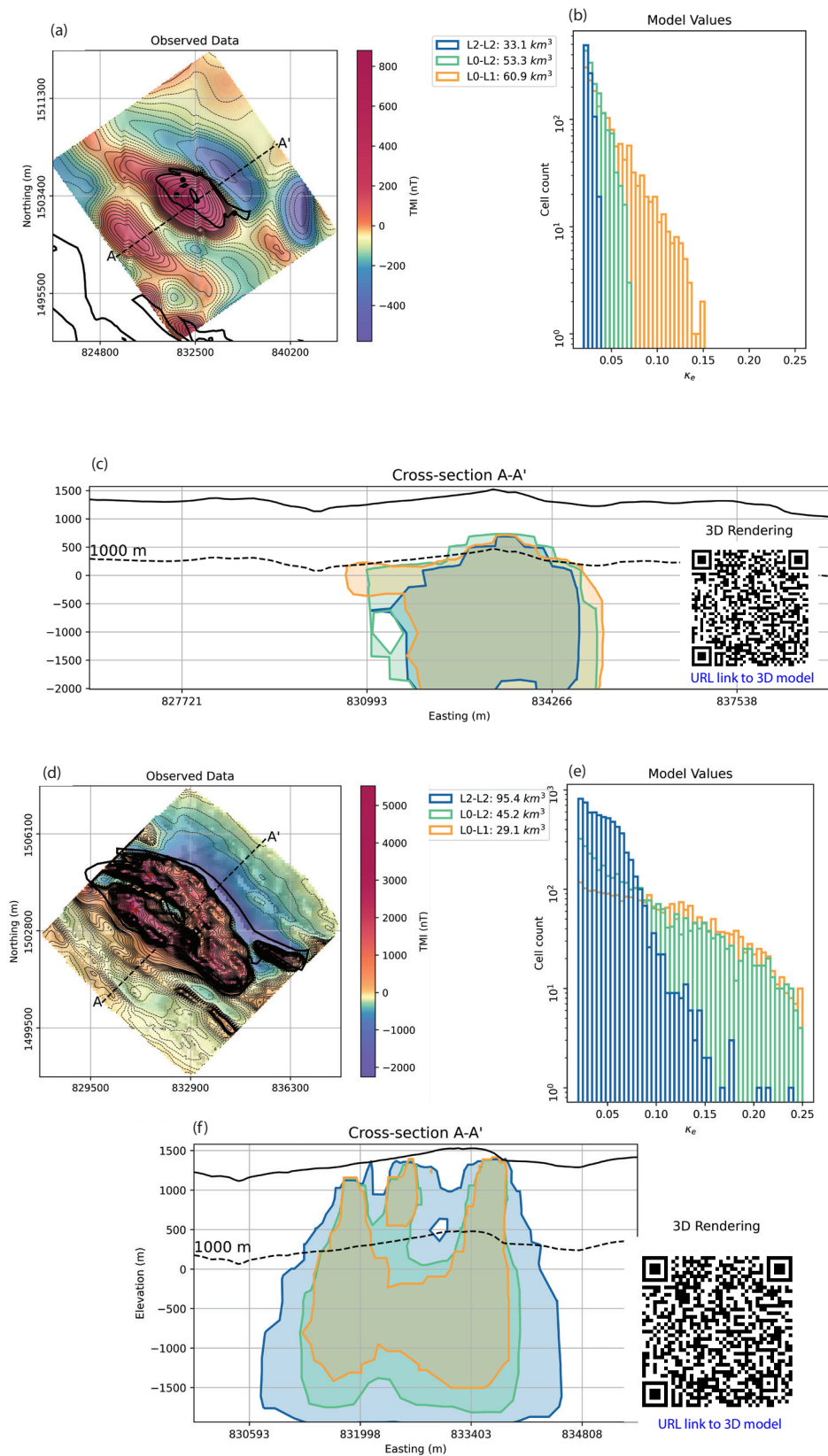


Figure 7: a-c) Inversion results for Turnagain using the NRCAN 200 m grid magnetic data, and d-f) the high resolution 100 m downsampled magnetic data. a) Observed NRCAN data over the Turnagain site; black dots are 'seeds' used to guide susceptibility volume cut-offs; b) effective susceptibility (K_e) ranges from the three model results; c) inversion results using the NRCAN magnetic data and three different ℓ_p norms - vertical section, showing the outlines of high effective susceptibility volumes where $K_e \geq 20 \times 10^{-3}$ SI; d) observed Aeroquest aeromagnetic data; e) effective susceptibility ranges from the three model results; f) inversion results using the Aeroquest magnetic data and three different ℓ_p norms - vertical section, showing the outlines of high effective susceptibility volumes where $K_e \geq 20 \times 10^{-3}$ SI. Scan the QR codes to view and manipulate the 3D model.

6.2 Decar site inversion of regional data to explore model outcomes

The Decar Nickel District is located 90 km northwest of Fort St. James, B.C. in the southern segment of the Cache Creek Terrane (Fig. 1) and hosts notable awaruite (Ni_3Fe) mineralization (Britten, 2017; Milidragovic et al., 2018; Milidragovic, 2019; Milidragovic and Grundy, 2019). The ultramafic rock package occurs as an oblong body elongated in the NW-SE direction that parallels the regional structural grain (Fig. 8). The rocks are variably serpentinized—although most are highly-serpentinized—and a belt of carbonated rocks (ophi-carbonate, soapstone, and listwanite) is inferred to occur along the central axis of the ultramafic body (Milidragovic et al., 2018; Milidragovic, 2019; Milidragovic and Grundy, 2019; Steinthorsdottir et al., 2020). Serpentinite density values directly correlate with degree of serpentinization and

the samples show the full range of magnetic susceptibilities, although typically they are relatively high ($>30 \text{ SI} \times 10^{-3}$). Carbonated rocks are mostly highly-carbonated and, as such, have relatively high densities ($\sim 2950\text{--}3000 \text{ kg/m}^3$) and low magnetic susceptibilities ($<20 \text{ SI} \times 10^{-3}$). Regions within the Decar site that preserve relatively fresh igneous minerals tend to show high natural remanent magnetization (NRM) and high Q-ratios (the ratio in a rock of remanent magnetization to the induced magnetization in the Earth's field) (Fig. 9); however, highly-serpentinized rocks locally also preserve high NRM and Q-ratio values. The relationship between NRM, Q-ratio, and degree of serpentinization will be further explored in the final report for this project.

An inversion of the Decar site using the 200 m gridded magnetic data from NRCan was completed to further assess the nature and range of inversion results from regional NRCan magnetic

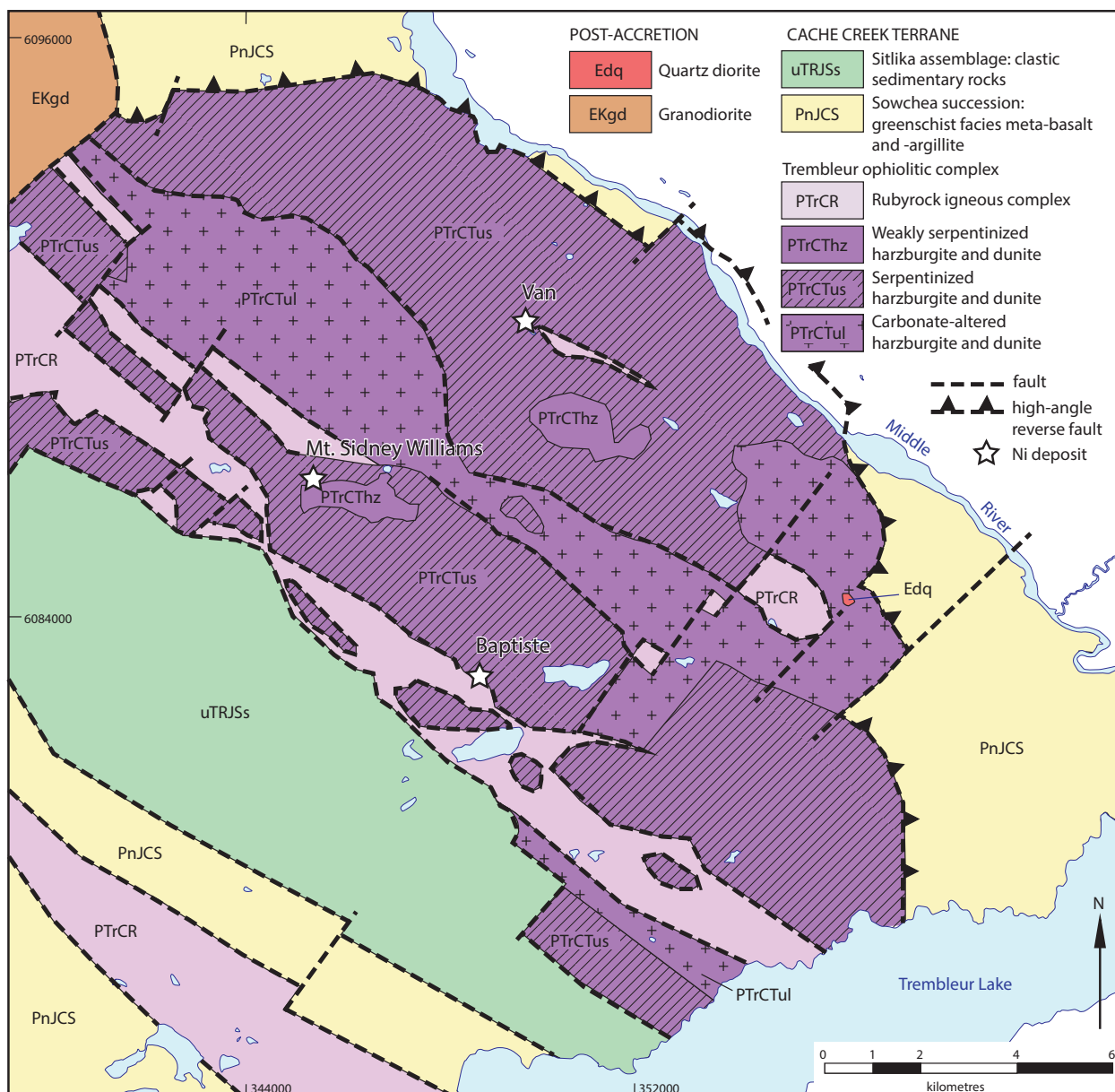


Figure 8: Decar area geology from Geology of the Cache Creek Terrane North of Trembleur Lake (modified from Milidragovic, 2019), the ultramafic locality 31 in Figure 1. Stars indicate mineralized locations. Coordinates are shown as NAD 83 UTM, Zone 10, units of metres.

data, which is to be used for most of the inversions planned for this project.

A range of ℓ_p norms were again applied to explore model possibilities (Fig. 10), and a lower bound effective magnetic susceptibility of 20×10^{-3} SI is used to represent the serpentinized volumes. The recovered volumes and range of susceptibilities vary with different applied norms. An L2-L2 norm leads to the smallest volume at a cut-off of 20×10^{-3} SI, and lowest range of susceptibilities, generally $<60 \times 10^{-3}$ SI. L0-L2 and L1-L1 norms result in larger volumes with higher susceptibilities up to and greater than 100×10^{-3} SI. The very high effective susceptibility outcomes using the L0-L2 and L1-L1 norm pairs are not consis-

tent with the lower expected ranges of susceptibility at Decar. This requirement for high susceptibilities of up to 250×10^{-3} SI to fit the observed data at Decar may indicate the presence of remanent magnetism at Decar, which is corroborated by a subset of rock samples that show elevated measured natural remanent magnetization and high Q-ratios (Fig. 9). The issues associated with the presence of remanent magnetization and its effect on predicted volumes of susceptibility is addressed in Section 6.3 through forward modeling tests.

Overall, the locations of the recovered high effective susceptibility volumes are similar, whether using the smoother L2 norms, or the more compact L0, and L1 norms, and this is reassuring

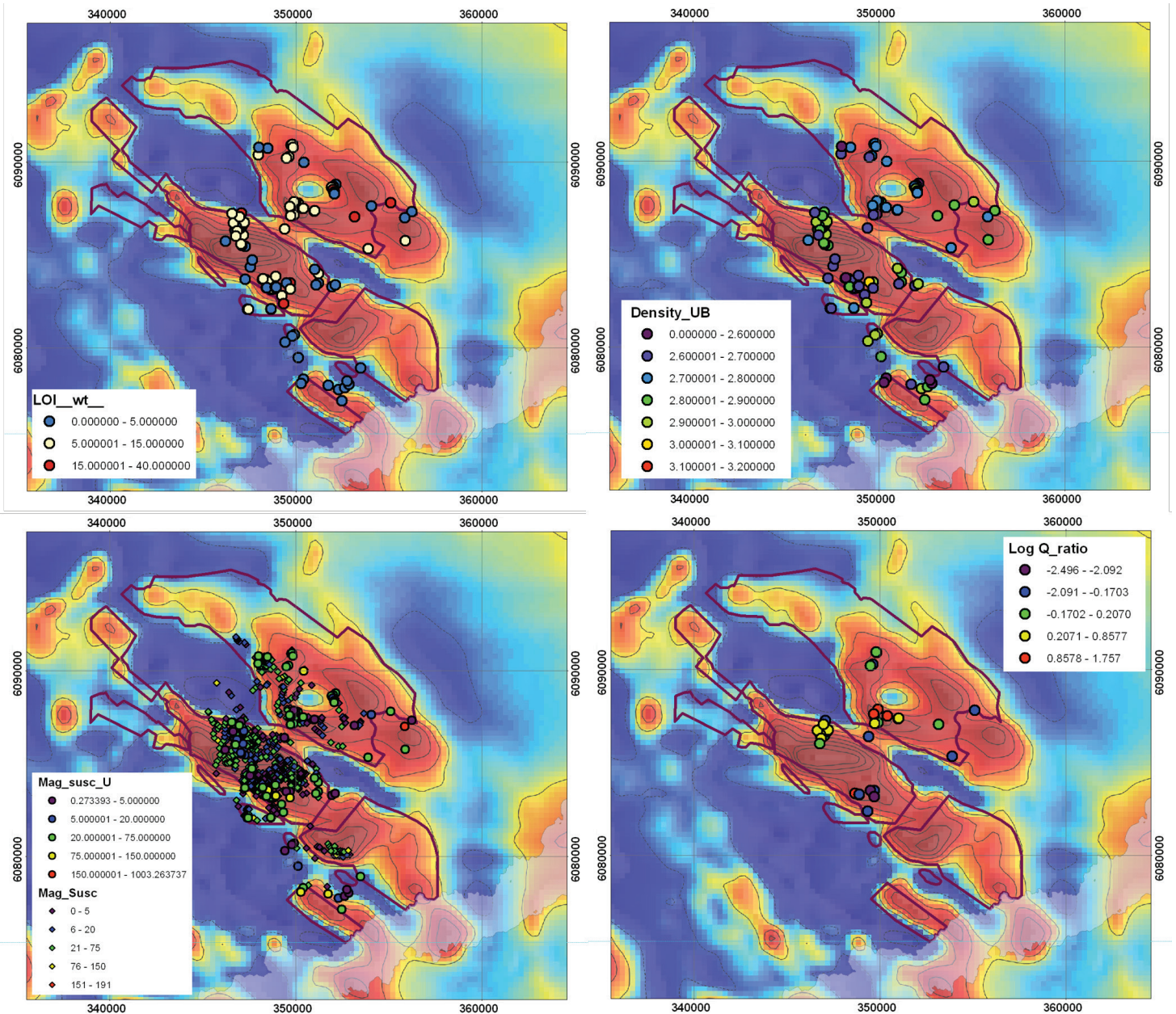


Figure 9: LOI and physical property data plotted on the magnetic grid from the Decar study area. The dark red outline represents mapped and interpreted serpentinized rocks. LOI data are binned based on trends seen in relation to serpentinization. LOI from 10–15 wt% is correlated with strongly serpentinized samples. These spatial plots show a correlation of low densities, $<2800 \text{ kg/m}^3$, and susceptibilities generally higher than 20×10^{-3} SI. Strong remanence in some areas is indicated by high Q-ratios. Coordinates are shown as NAD 83 UTM, Zone 10, units of metres.

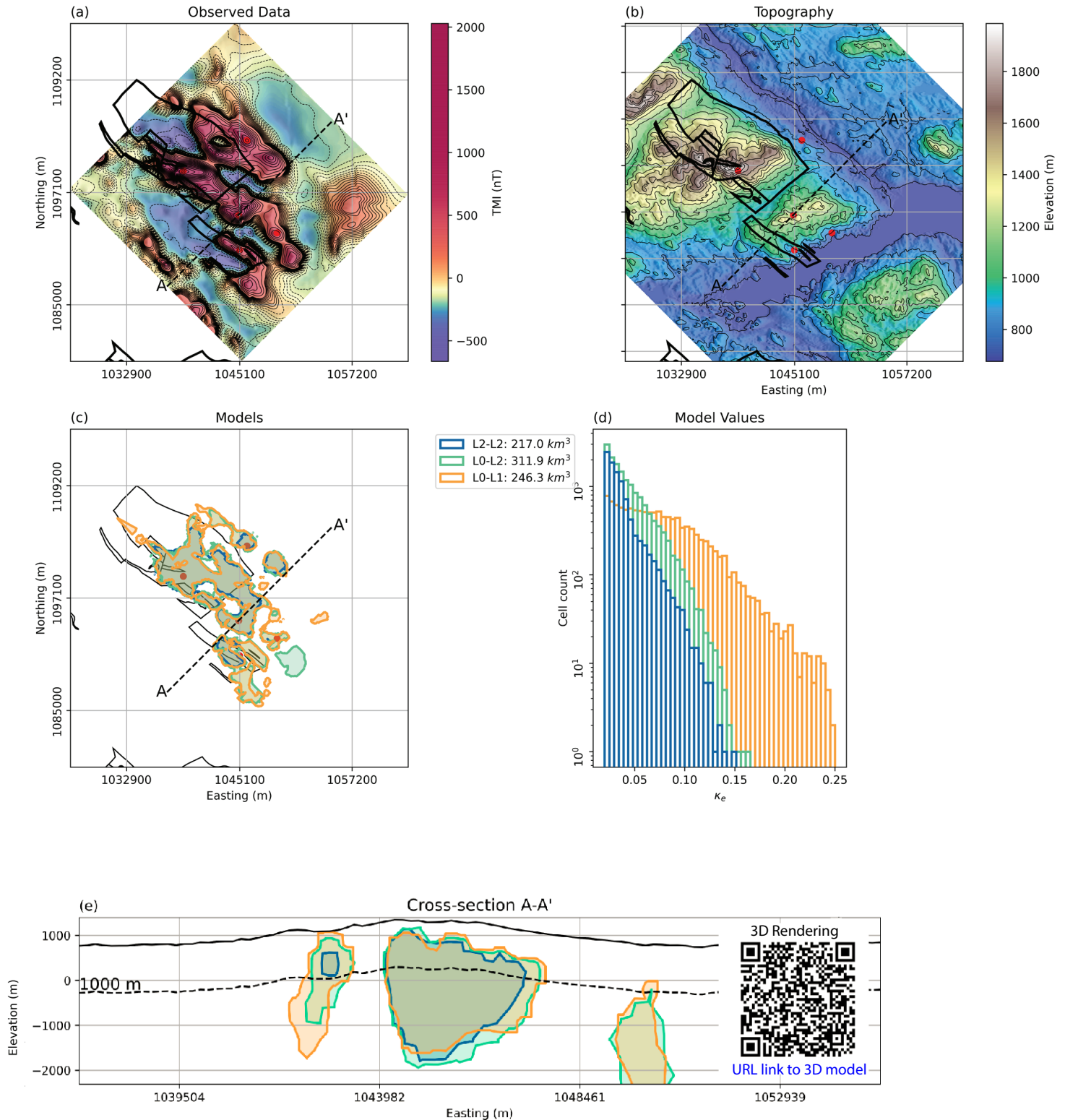


Figure 10: Inversion of the NRCAN 200 m grid magnetic data over Decar. **a)** observed NRCAN data with magnetic anomaly 'seeds' (red points) used to guide susceptibility volume cut-offs; **b)** topography; **c)** inversion results using the NRCAN 200 m grid magnetic data and three different ℓ_p norms - horizontal section, showing the outlines of high effective susceptibility (K_e) volumes where $K_e \geq 20 \times 10^{-3}$ SI; **d)** effective susceptibility (K_e) ranges from the three model results; **e)** inversion results using the NRCAN 200 m grid magnetic data and three different ℓ_p norms - vertical section, showing the outlines of high effective susceptibility volumes where $K_e \geq 20 \times 10^{-3}$ SI. Scan the QR code to view and manipulate the 3D model.

in terms of there being a consistent distribution of high effective susceptibility zones. As with the Turnagain inversions, the inversion of regional aeromagnetic datasets tends to push the resolved serpentinite bodies to depth. This is inconsistent with the prevalence of serpentinite at, and immediately below, the surface as documented by mapping and extensive exploration drilling (Britten, 2017; Milidragovic, 2019; Steinhorsdottir et al., 2020).

6.3 Decar site forward modelling simulation

Several forward and inverse modeling simulations were completed to investigate whether it is possible to match the magnetic data at Decar to the observed geology and measured magnetic susceptibilities, and to determine how well a known volume can be recovered.

Building from the SimPEG package (Cockett et al., 2015), an open-source application, which allows users to define a geophysical survey area, and move and change the size, shape, and orientation of blocks that mimic magnetically susceptible bodies, was developed for forward modeling of magnetic data. A 3D block model was built to approximate the distribution of high-susceptibility material at Decar with additional volumes representing background rocks (Fig. 11). Magnetic susceptibilities of 'serpentinized' volumes were set with an upper bound of 80×10^{-3} SI based on the Q3 value of the full ophiolite sample set. A constant inducing magnetic field was applied to those blocks to simulate the local conditions. In this case, the applied magnetic field parameters approximate Earth's magnetic field at the Decar site. The simulated magnetic data from this model are shown with true observed Decar magnetic data (Fig. 12a,b).

An important observation made during this forward simulation was that the amplitude of the highest observed magnetic anomalies could not be achieved using blocks of magnetic susceptibility at 80×10^{-3} SI, which is representative of the upper range of magnetic susceptibility values typical for serpentinized rocks in the Decar area. In an effort to try to create larger susceptibility volumes to fit the data, the base of select blocks was moved progressively deeper, yet the amplitude was still not achieved. In fact, large volumes with susceptibilities greater than 250×10^{-3} SI, values rarely seen in collected samples, would be required to fit the observed data. In addition, the large negative lobe in the northwest quadrant of the data (Fig. 12b), could not be replicated by the forward simulation. The strongly negative field here is inconsistent with what might be expected of a steep (near vertical) inducing field at this latitude. The difficulty in fitting these high and low values demonstrates that a remanent component of magnetization needs to be considered to simulate the magnetic responses at the Decar site.

With the synthetic Decar model we have the opportunity to assess the accuracy of volumes recovered by 3D inversion using the MVI code, since we know the true volume of the high susceptibility rocks. The simulated magnetic data (Fig. 12a) were

inverted to recover estimates of the total volume, position, and shape of the high susceptibility blocks. The inversion of the simulated magnetic data using a lower bound magnetic susceptibility threshold of 20×10^{-3} SI resulted in high effective magnetic susceptibility volumes ranging from 46–65 km³ (Fig. 12c,e). The true model block volume in the synthetic model is 78 km³. The resulting effective susceptibility values were slightly underestimated at less than 60×10^{-3} SI, compared to the susceptibilities of 80×10^{-3} SI assigned to the model blocks (Fig. 12d). There is a reasonable match between the locations and depths of the recovered high susceptibility domains and the original block model.

Forward modeling and inversion of the synthetic Decar model yielded three important results. Firstly, our inability to match the amplitude of the observed magnetic field data from Decar, based on existing knowledge of physical properties and geology at Decar, suggests that magnetic remanence is a significant contributor to the overall magnetic response. Secondly, the effective susceptibilities recovered using inversion consistently underestimate the actual physical properties of the rocks. This is generally expected from unconstrained geophysical inversions. Thirdly, the simulated data inversion shows that under optimal conditions we can obtain reasonable approximations of the position, shape, and size of susceptible bodies using magnetic data gridded at approximately 275 m and at 300 m elevation, data parameters adopted from the national NRCan magnetic dataset.

7. VOLUME ESTIMATION OF SERPENTINIZED ROCK AT SELECT LOCALITIES USING MAGNETIC INVERSION

The detailed inversions at Turnagain and Decar have informed an approach to inverting regional NRCan data for other ultramafic occurrences in B.C. where detailed mapping and drilling data are less complete. Nine ultramafic sites were selected out of a total of 49 for an initial assessment of serpentinite volume using 3D magnetic inversion modeling (Fig. 13). These localities represent some of the more significant and well-known ultramafic rock districts in the province. A total of 21 inversions capturing distinct magnetic anomalies were completed over the nine localities. The inversion process was the same as used for detailed analysis at Turnagain and Decar, and the same range of ℓ_p -norm models was included. We can anticipate from using the NRCan 200 m gridded magnetic data for the site-specific case studies that these inversions are capable of recovering the size and shape of high-susceptibility serpentinized zones, but that the location of the central mass of the bodies may be migrated to greater depth than expected for these ultramafic units with confirmed surface exposure. The contribution of remanent magnetism is also not resolved at this time. For these inversions, lower threshold values for magnetic susceptibility (20×10^{-3} SI) are used but the upper bounds are not constrained.

Representative map sections through each of the 21 sites are

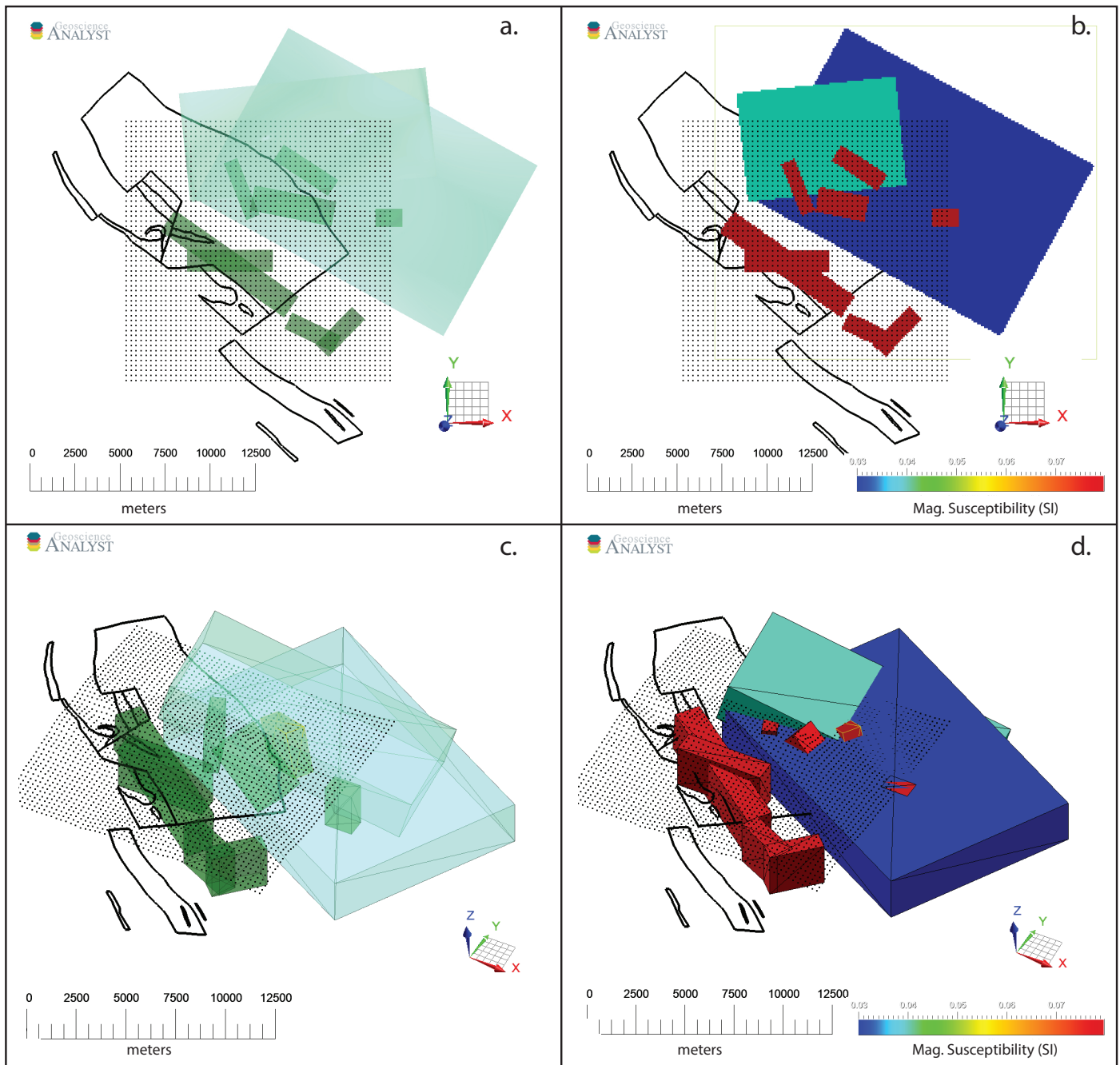


Figure 11: Map view (a,b) and perspective view (c,d) of 3D blocks used to simulate the magnetic data from the Decar area. The images on the left (a,c) show high susceptibility 'serpentinized' blocks in dark green and lower susceptibility material required by the model in light green. The images on the right (b,d) show the model blocks painted by their assigned magnetic susceptibility values. The colorless volume outside the model blocks is 'background' and assigned a magnetic susceptibility of 0 SI. Black outlines are the ultramafic rock polygons from the BCGS bedrock geology database. Black points represent the grid for the simulated magnetic survey.

presented in Figure 14 along with total volumes of each of the three models, generated using different ℓ_p -norms. For comparison, the median volume for each locality is presented in Table 3. These data show that the inverted serpentinite rock volumes do not closely match volumes estimated from direct extrapolation of co-located polygon areas to depth. The total volume of serpentinitized rock based on polygon extents and assuming the thickness of 0.5 km is 675 km³, whereas the total volume derived from inversion modeling using a depth cut-off of 0.5 km is only 102 km³. This discrepancy reflects at least two sources of error.

Firstly, the inversion of regional NRCan geophysical data erroneously pushes the location of susceptible bodies to depth, as seen in examples from Turnagain (Fig. 7) and Decar (Fig. 10) where mapping and mineral exploration drilling has confirmed large volumes of serpentinitized rock near surface (<0.5 km depth). This leads to an underestimation of susceptible material near surface. Secondly, a simple vertical extension of mapped rock boundaries from the surface to depth is unlikely to represent a reasonable extrapolation of either the ophiolitic thrust-sheets or intrusive ultramafic rock bodies, and it assumes the unit is

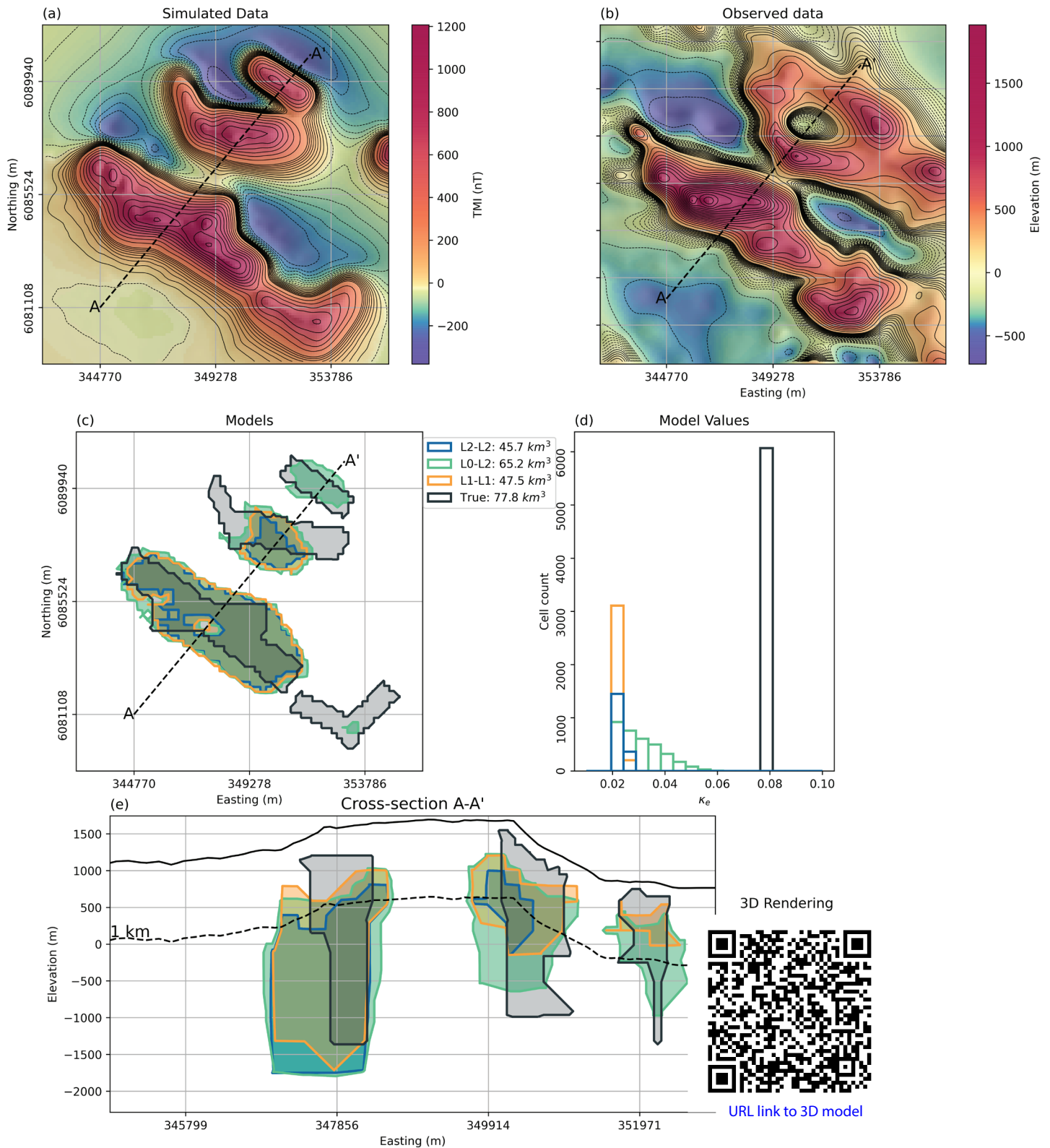


Figure 12: Inversion of simulated data from the synthetic Decar block model to compare recovered volumes. **a)** simulated magnetic data generated from the synthetic Decar model; **b)** observed NRCAN TMI data; **c)** inversion results using the simulated magnetic data and three different ℓ_p norms - horizontal section, showing the outlines of high effective susceptibility (K_e) volumes where $K_e \geq 20 \times 10^{-3}$ SI, and the outlines of the original blocks; **d)** effective susceptibility ranges from the three model results compared to the original starting model; **e)** inversion results using the simulated magnetic data and three different ℓ_p norms - vertical section showing the outlines of high effective susceptibility volumes where $K_e \geq 20 \times 10^{-3}$ SI.

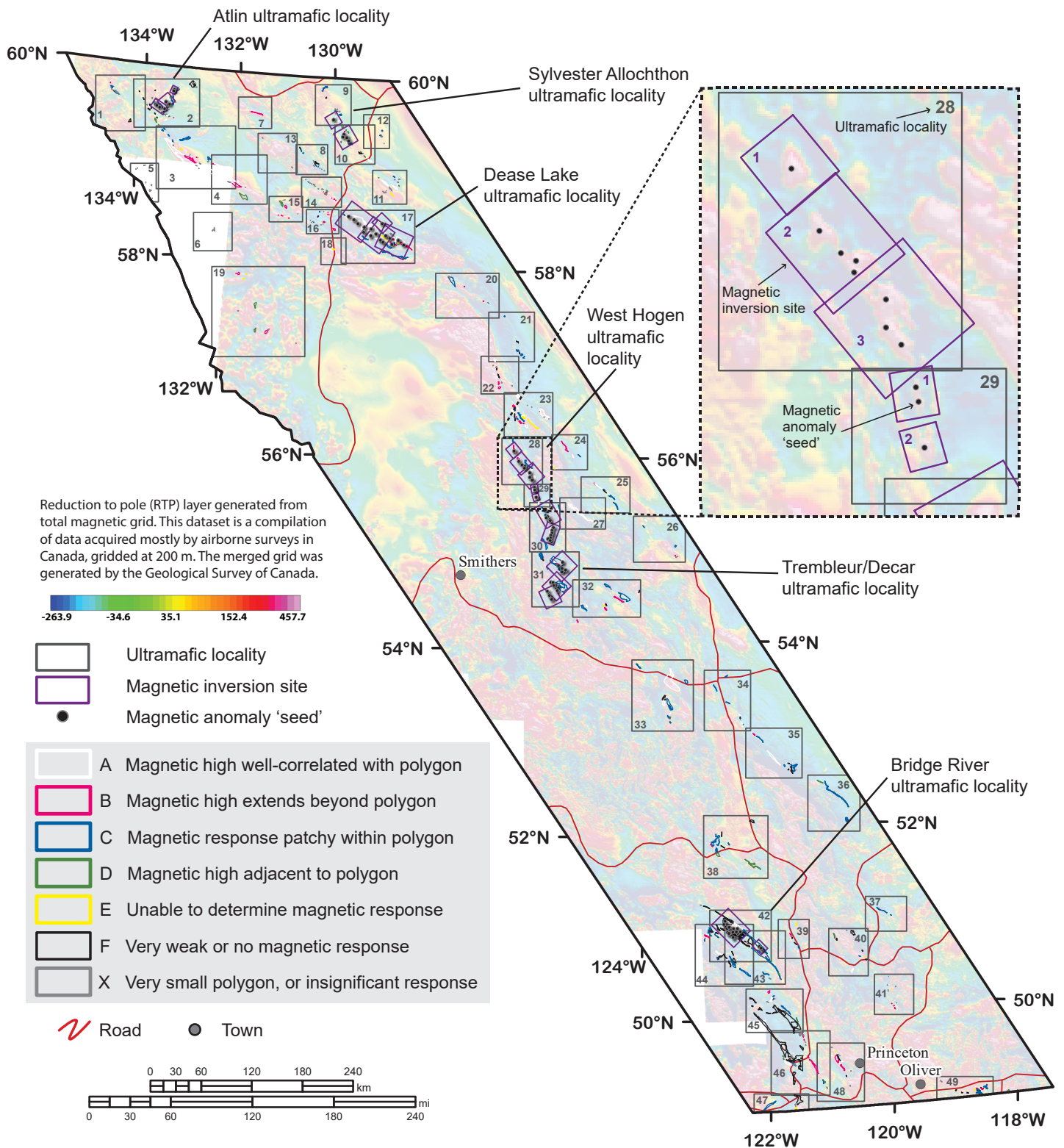


Figure 13: Locations of ultramafic sites chosen for preliminary inversion modeling. Inset from the West Hogen Batholith area illustrates an example of how magnetic inversion sites (purple polygons) were chosen within localities 28 and 29. Black points within each inversion site are the magnetic anomaly 'seeds' used to anchor volume calculations.

homogeneously serpentinized. Because of this, volume calculations directly from polygons are likely overestimated. Although high susceptibility masses are expected to reach the surface in most cases based on geological mapping and available rock property measurements, the results of NRCan magnetic data inversions regularly, but not always, place the masses deeper, meaning that there are significant jumps in volume estimations from 0.5 km to 1 km, and then to 2 km. The total volume of serpentinized rock for the 21 sites is 3,769 km³ of which 47% (1,754 km³) is estimated to reside within 2 km of the surface. There is still a large portion of the modelled volume deeper than 2 km. Extension of ultramafic rock bodies vertically to depths greater than 2–3 km is not generally consistent with shallow thrust sheet geometries that are often inferred for ophiolite-type ultramafic rock bodies in B.C. where drill data and exposures have demonstrated the depth limits of these bodies are generally shallower. Although the placement of the susceptible mass is suspect, low- and high-resolution data inversion comparisons at Turnagain, and synthetic modeling at Decar provides some confidence that recovered volumes are reasonably estimated using susceptibility thresholds informed by physical property data analysis. Future work will focus on exploring inversion constraints' effect on placement of recovered bodies, and validation of volume estimates where geological observations or other higher resolution data exist.

The total area of ultramafic polygons captured by inversions from 21 site localities is 1,351 km², equaling slightly less than half of the area estimated from all A, B, and C ranked polygons (total area 2,871 km²). A preliminary estimate of the total volumes of serpentinite in B.C. was obtained by extrapolating the inversion results summarized in Table 3 proportionally to the full areal extent of A, B and C ranked polygons. The estimated volumes are included in the last row of Table 3. The total volume of serpentinized rock within 1 km of the surface is estimated to be 988 km³. This represents only 34% of the volume based on vertical extrapolation of polygon areas (2871 km³; Section 5). The discrepancy reflects both the incomplete serpentinization with-

in these rock bodies as well as the artificial projection to depth of the magnetic anomalies by the models when using the coarse regionally gridded magnetic data. The total volume of serpentinites within 2 km of the surface is estimated to be 3736 km³.

8. DISCUSSION

The thickness and subsurface extension of most ultramafic rock bodies in B.C. is poorly constrained by surface geology. We instead rely on inversion modeling of magnetic anomalies to estimate the volume of serpentinized ultramafic rock. Although the coarse resolution of regional magnetic data for B.C. complicates this, as does the contribution of magnetic remanence, our ability to image and quantify the abundance of ultramafic rocks for carbon mineralization is nonetheless markedly improved compared to simple vertical extrapolation of surface geological relationships.

Two modes of carbon mineralization within ultramafic rocks can be envisaged. *Ex-situ* mineralization would rely on the extraction of reactive ultramafic rocks from an open pit or underground mine, and processing for both metal (e.g., Ni) recovery as well as carbon mineralization. It is feasible with existing technology and has been documented in the tailings storage facilities of operating nickel and diamond mines in Canada and Australia (Power et al., 2013). Alternatively, Kelemen and Matter (2009) have proposed injection of CO₂ into subsurface ultramafic rocks to drive *in-situ* carbon mineralization in a process akin to what has been achieved in mafic rocks at Carbfix in Iceland (Snæbjörnsdóttir et al., 2020). The injectivity and fast reaction rates needed to sustain *in-situ* carbon mineralization have not been demonstrated in ultramafic rocks to date.

Mining for *ex-situ* mineralization would necessarily be restricted to shallow ultramafic rock bodies with a depth limit of about 1 km. Mineralization is considered readily achievable at relatively low cost using existing technologies if only the highly reactive labile fractions of the ultramafic body are targeted (Wilson et al., 2014; Lu, 2020). The downside of targeting only the highly reac-

Table 3: Model areas and volumes of serpentinized ultramafic rocks by locality.

Locality Name	Ultramafic Locality	Polygon area captured by inversion sites - A, B, C only	Volume related to polygons (assuming 0.5 km thick)	High sus volume from inversions (top 0.5 km - median)	High sus volume from inversions (top 1 km - median)	High sus volume from inversions (top 2 km - median)	High sus volume from inversions (top 4 km - median)	High sus volume from inversions (full depth median)
Unit		km ²	km ³	km ³	km ³	km ³	km ³	km ³
Atlin	2	60	30	6	21	50	56	56
Sylvester Allochthon	9	8	4	0	2	8	13	13
Sylvester Allochthon	10	54	27	1	11	43	57	57
Dease Lake	17	413	207	4	88	596	1375	1414
West Hogem Batholith	28/29	168	84	26	89	267	534	534
West Hogem Batholith	30	100	50	12	42	143	354	354
Trembleur/Decar	31	248	124	37	153	449	826	840
Bridge River	42	299	150	17	58	199	493	501
Totals		1351	675	102	464	1754	3708	3769
Factor of 2.13 to give total A, B, C polygons for BC		2878 km ²	1438 km ³	218 km ³	988 km ³	3736 km ³	7898 km ³	8028 km ³

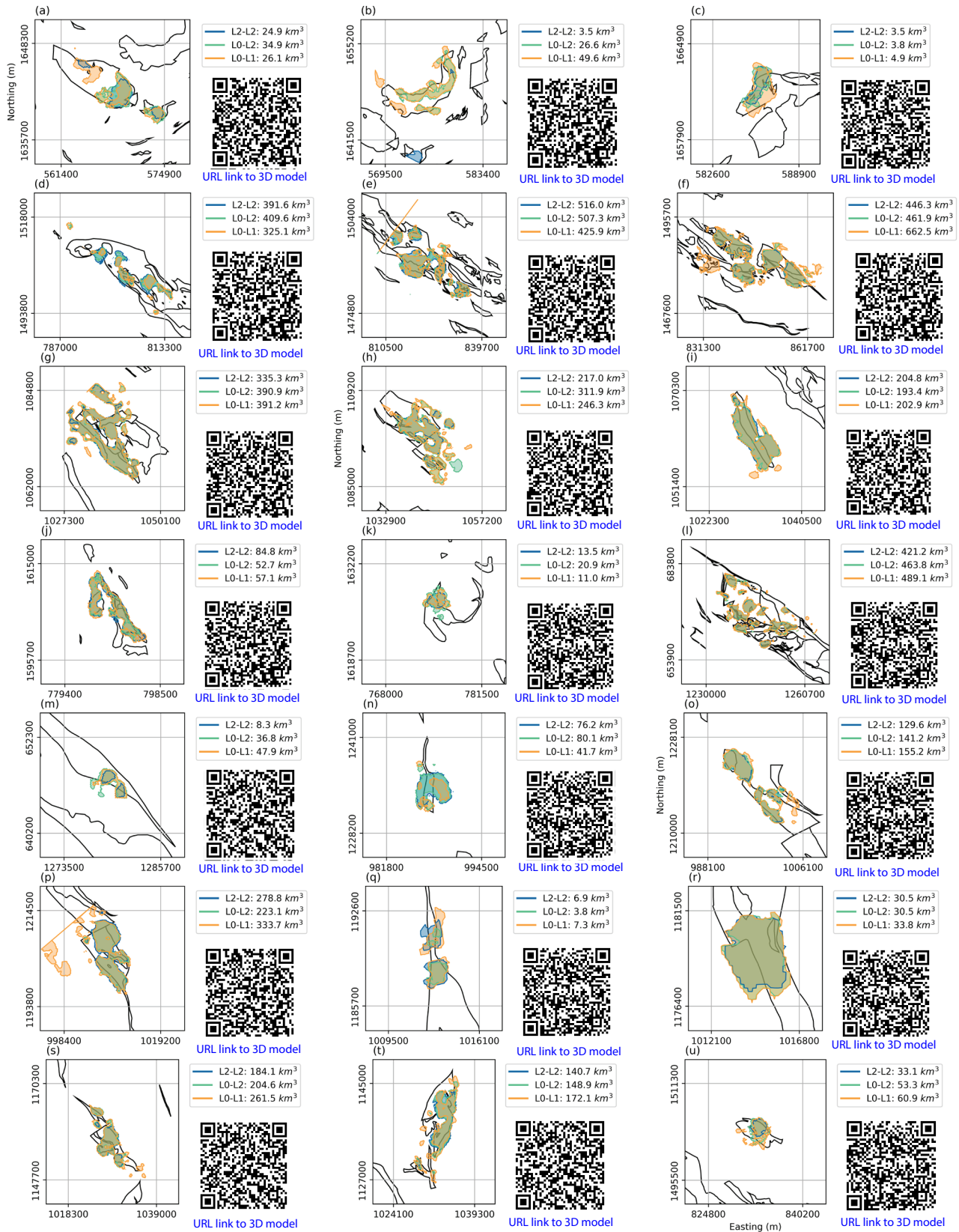


Figure 14: Inversion results using the NRCan magnetic data and three different ℓ_p norms - horizontal sections, showing the outlines of high susceptibility volumes where susceptibility (K_s) is $\geq 20 \times 10^3$ SI. **a)** Locality 2 (Atlin) - inversion 1; **b)** Locality 2 (Atlin) - inversion 2; **c)** Locality 2 (Atlin) - inversion 3; **d)** Locality 17 (Dease Lake) - inversion 1; **e)** Locality 17 (Dease Lake) - inversion 2; **f)** Locality 17 (Dease Lake) - inversion 3; **g)** Locality 31 (Decar area) - inversion 1; **h)** Locality 31 (Decar area) - inversion 2; **i)** Locality 31 (Decar area) - inversion 3; **j)** Locality 10 (Sylvester Allochthon) - inversion 1; **k)** Locality 9 (Sylvester Allochthon) - inversion 1; **l)** Locality 42 (Bridge River) - inversion 1; **m)** Locality 42 (Bridge River) - inversion 2; **n)** Locality 28 (West Hogem) - inversion 1; **o)** Locality 28 (West Hogem) - inversion 2; **p)** Locality 28 (West Hogem) - inversion 3; **q)** Locality 29 (West Hogem) - inversion 1; **r)** Locality 29 (West Hogem) - inversion 2; **s)** Locality 30 (West Hogem) - inversion 1; **t)** Locality 30 (West Hogem) - inversion 2; **u)** Locality 17 (Dease Lake/Turnagain) - inversion 4.

Table 4: Serpentinite volume and carbon sequestration capacity for all of B.C. based on data from Table 3.

Depth Interval (km)	Serpentinite Volume (km ³)	Sequestration Capacity (Gt CO ₂)	Method
0 to 1	988	56	<i>ex-situ</i>
0 to 2	3,689	210	<i>ex-situ</i>
2 to 4	4,162	5,139	<i>in-situ</i>
2 to full depth	4,292	5,300	<i>in-situ</i>

tive ultramafic rocks is that it only uses a small fraction of the total Mg content of the ultramafic rock. Relevant data on labile Mg of serpentinized ophiolitic rocks from B.C. are available for the Decar area from Vanderzee et al. (2019) who estimated the average to be 2.3 wt% MgO for the one billion tonne Baptiste Ni deposit. Applying this average labile Mg content, assuming a bulk density of 2800 kg/m³ (Fig. 2) for serpentinite, and conversion to solid mineral carbonate with hydromagnesite mineral stoichiometry, a sequestration conversion factor of 0.0563 Gt CO₂ per km³ of serpentinite is obtained.

The total carbon sequestration capacity for mineralization of serpentinite volumes using various depth cut-offs is listed in Table 4. Using a cut-off of 1 km depth, we estimate that the carbon sequestration capacity for *ex-situ* mineralization in B.C. is on the order of 56 Gt of CO₂. This represents roughly 800 years' worth of B.C.'s total GHG emissions (as CO₂ equivalent) based on reported 2018 rates of 68 Mt CO₂ annually. Volumes, and thus carbon sequestration capacity, coinciding with a cut-off of 1 km likely represents a minimum value because as discussed above, inversion of regional magnetic data pushes the core of recovered high susceptibility masses to depths of 1–3 km, even where we know that high susceptibilities occur at surface (Figs. 7, 10, 12). A much larger capacity, 210 Gt CO₂ or 3,000 years of B.C. emissions representative of the volumes to a depth of 2 km, would capture that missing capacity but likely also overestimates the volumes of ultramafic rock. Future work investigating how mass is distributed through inversion of coarse regional magnetic data will lead to more confident determinations of whether high susceptibility serpentinized rock is physically accessible and economically viable. Until that work is complete, we focus on the more conservative estimate derived from only considering the top 1 km. It is neither suggested nor anticipated that all of these serpentinites will be mined. Rather, this represents a substantial resource which should be further evaluated for opportunities to combine carbon sequestration activities with resource development, especially for critical metals that will be needed for the decarbonization of the electricity and transportation sectors.

In-situ carbon mineralization is envisaged to convert all Mg in ultramafic rock to magnesite but relies on processes such as reaction-driven cracking which have not been demonstrated under field conditions. Kelemen et al. (2020) further explore the assumptions and some of the anticipated costs for *in-situ* carbon mineralization should this process ultimately be shown

to be technically feasible. *In-situ* mineralization would inject CO₂ to depths of 2 km or more, where the ambient temperature and pressure are optimal for rapid reaction kinetics (Kelemen and Matter, 2009). The geophysical inversions presented here estimate the volume of ultramafic rocks at this depth interval to be 4,292 km³ although we recognize that this again may be a significant overestimation due to: 1) the current uncertainties in the role of magnetic remanence, and 2) the coarse resolution, and mass distribution using regional magnetic surveys. Nonetheless, this volume represents a CO₂ sequestration capacity of more than 5,000 Gt (Table 4), assuming full carbonation. *In-situ* mineral carbonation applies to both fresh ultramafic igneous rocks as well as serpentinites. The effectiveness of *in-situ* mineral carbonation in partially carbonate altered ultramafic rocks has not been assessed but can be expected to be reduced over that in serpentinites and fresh igneous rocks. The geophysical inversions developed here and based on high magnetic susceptibility preferentially identify zones of serpentinization and will not include fresh igneous rocks or highly carbonate altered rocks. Thus, to the extent that fresh ultramafic igneous rocks persist at depth, the capacity for in-situ carbon mineralization would be greater than that reported here.

9. SUMMARY

The development of a new physical properties model for ultramafic igneous rocks and their altered equivalents, together with the integration and reinterpretation of publicly available bedrock geology and airborne geophysical data, demonstrate the large potential for the capture and storage of CO₂ within serpentinized ultramafic rock bodies in B.C. Uncertainties related to the compilation and gridding of legacy aeromagnetic data results in geophysical models that artificially push the location of the rock bodies to depth. Nonetheless, reasonable approximations in size and shape of serpentinized zones can be retrieved. Results indicate that approximately 75% of the ultramafic rocks in B.C. are serpentinized and that the volumes of serpentinized rocks are only about 34% of that estimated by vertically projected surface map polygons to depths of 1 km. Based on the leachable magnesium content of serpentinite in the Decar area, this volume if mined and allowed to react with CO₂ in the atmosphere could mineralize 800 years' worth of B.C.'s GHG emissions. The capacity is likely greater than this because the geophysical models place the bulk of the mass of serpentinized rock to depths

greater than 1 km yet detailed observation and drill data, where available, demonstrate they occur at and near the surface. Further refinements to the geophysical models will aim to reduce this discrepancy. The volume of ultramafic rock at depths greater than 2 km, which might be used for *in-situ* carbon mineralization, are much larger (>5,000 Gt CO₂ capacity), however, this estimate of the amount of serpentinite at depth may be too large due to the same bias in the geophysical models.

10. FUTURE WORK

The CaMP-BC project will conclude with a final report in early 2021. For that report, further refinements to the inversion models deployed here will evaluate key uncertainties. This will include the inversion of NRCAN magnetic data (or higher resolution data where available) at 49 localities and an estimate of total CO₂ sequestration capacity by ultramafic rocks in B.C. Work will also address the extent to which remanence plays a role in the observed magnetic response and the resulting modelled inversion volumes. Depth weighting and levelling issues, possibly causing deep placement of susceptibility masses when inverting using NRCAN data, will be further explored. To guide future work, such as serpentinitization assessments, magnetic modeling, and ultramafic rock exploration target selection, an Atlas of Magnetic Responses of Ultramafic Rocks in B.C. is being compiled. A total of 49 paired maps will be compiled that show geologic terranes and magnetic data for each ultramafic locality. Minfile occurrences will indicate where past and active mines exist, and where exploration for ultramafic rock hosting mineral deposits has occurred.

Despite these refinements, significant sources of error will remain in the estimates of the carbon mineralization potential largely because of the uncertainties associated with variable contributions of magnetic remanence and due to the coarse resolution of the NRCAN regional magnetic datasets. Future work to improve geophysical inversions will include evaluation of magnetic remanence at specific localities, and inversion of higher resolution magnetic and gravity data for improved serpentinite mapping and volume estimation. These investigations will also evaluate the ability to resolve the extent of ultramafic bodies to depths greater than 2 km, which is necessary to assess the potential for *in-situ* mineralization.

11. ACKNOWLEDGEMENTS

This research was funded by Geoscience B.C. through project 2018-038. The B.C. Geological Survey supported participation of D.M.; A.N. was supported in part by a Student Work Placement Program funded by Employment and Social Development Canada. FPX Nickel Corp and GigaMetals provided data and rock samples from the Decar and Turnagain nickel deposits. The manuscript was greatly improved by the thorough comments of three anonymous reviewers. A. Zagorevski (GSC-NRCAN) provided

samples for the Nahlin, King Mountain, southern Yukon, and some Atlin samples; these were collected as part of the Geological Survey of Canada's Geo-mapping for Energy and Minerals programs. Bethany Ladd provided images and graphics. Shannon Guffey and Sara Jenkins assisted with final figures and layout.

12. REFERENCES

- Bonnemains, D., Charlut, J., Escartín, J., Mével, C., Andreani, M., & Debret, B. (2016). Magnetic signatures of serpentinitization at ophiolite complexes. *Geochemistry, Geophysics, Geosystems*, 17(8), <https://doi.org/10.1002/2016GC006321>
- Britten, R. (2017). Regional metallogeny and genesis of a new deposit type—Disseminated awaruite (Ni₃Fe) mineralization hosted in the Cache Creek Terrane. *Economic Geology*, 112, 517–550. <https://doi.org/10.2113/econgeo.112.3.517>
- Cockett, R., Kang, S., Heagy, L., Pidlisecky, A., & Oldenburg, D. (2015). SimPEG: An open source framework for simulation and gradient based parameter estimation in geophysical applications. *Computers & Geosciences*. 85, 142–154. <https://doi.org/10.1016/j.cageo.2015.09.015>
- Cui, Y., Miller, D., Schiarizza, P., & Diakow, L.J., 2017. British Columbia digital geology. British Columbia Ministry of Energy, Mines and Petroleum Resources, British Columbia Geological Survey Open File 2017-8, 9p. Data version 2019-12-19.
- Cutts, J., Dipple, G.M., Hart, C.J.R., & Milidragovic, D. (2020). Assessment of the carbon mineralization potential of British Columbia by quantifying the response of physical properties to the alteration of ultramafic rocks (NTS 092H/08, 10, 093K/13, 14, 094C/05, 104I, 104N). *In: Geoscience BC Summary of Activities 2019: Minerals*, Geoscience BC, Report 2020-01, p. 137–144.
- Deschamps, F., Godard, M., Guillot, S., & Hattori, K. (2013). Geochemistry of subduction zone serpentinites: A review. *Lithos*, 178, 96–127. <https://doi.org/10.1016/j.lithos.2013.05.019>
- English, J. M., Mihalyuk, M. G., & Johnston, S. T. (2010). Geochemistry of the northern Cache Creek terrane and implications for accretionary processes in the Canadian Cordillera. *Canadian Journal of Earth Sciences*, 47, 13–34. <http://https://doi.org/10.1016/j.lithos.2018.06.001>
- Fournier, D. & Oldenburg, D.W. (2019). Inversion using spatially variable mixed ℓ_p norms. *Geophysical Journal International*, 218, 268–282, <https://doi.org/10.1093/gji/ggz156>
- Hancock, K.D. (1990). Ultramafic associated chromite and nickel occurrences in British Columbia. British Columbia Ministry of Energy, Mines and Petroleum Resources, Mineral Resources Division, Geological Survey Branch. Open File 1990-27, 1–62.
- Hansen, L. D., Dipple, G. M., Gordon, T. M., & Kellett, D. A. (2005). Carbonated serpentinite (listvenite) at Atlin, Brit-

- ish Columbia: a geological analogue to carbon sequestration. *The Canadian Mineralogist*, 43, 225–239. <https://doi.org/10.2113/gscanmin.43.1.225>
- Hostetler, P. B., Coleman, R. G., & Evans, B. W. (1966). Brucite in alpine serpentinites. *American Mineralogist*, 51, 75–98.
- Jackson-Brown, S., Scoates, J.S., Nixon, G.T., & Ames, D.E. (2014). Mineralogy of sulphide, arsenide, and platinum-group minerals from the DJ/DB zone of the Turnagain Alaskan-type ultramafic intrusion, north-central British Columbia. *In: Geological Fieldwork 2013*, British Columbia Ministry of Energy of Mines, British Columbia Geological Survey Paper 2014-1, 157–168.
- Kelemen, P. B. & Matter, J. (2009). *In situ* carbonation of peridotite for CO₂ storage. *Proceedings of the National Academy of Sciences*, 105(45), 17295–17300. <https://doi.org/10.1073/pnas.0805794105>
- Kelemen, P.B., Matter, J., Streit, E.E., Rudge, J.F., Curry, W.B., & Blusztajn, J. (2011). Rates and Mechanisms of Mineral Carbonation in Peridotite: Natural Processes and Recipes for Enhanced, *in situ* CO₂ Capture and Storage. *Annual Review of Earth and Planetary Sciences*, 39:1, 545–576.
- Kelemen, P.B., McQueen, N., Wilcox, J., Renforth, P., Dipple, G., & Paukert Vankeurene, A., (2020). Engineered carbon mineralization in ultramafic rocks for CO₂ removal from air: Review and new insights. *Chemical Geology*, 550, 119628. <https://doi.org/10.1016/j.chemgeo.2020.119628>
- Krevor, S.C., Graves, C.R., Van Gosen, B.S., & McCafferty, A.E. (2009). Mapping the mineral resource base for mineral carbon-dioxide sequestration in the conterminous United States: U.S. Geological Survey Data Series 414, 14 p., 1 pl., scale 1:5,000,000. <https://pubs.er.usgs.gov/publication/ds414>
- Kump, L.R., Brantley, S.L., & Arthur, M.A. (2000). Chemical weathering, atmospheric CO₂, and climate. *Annual Review of Earth and Planetary Sciences*, 28, 611–667.
- Lackner, K.S. (2003). Climate change: A guide to CO₂ sequestration. *Science*, 300, 1677–1678.
- Lackner, K. S., Butt, D. P., & Wendt, C. H. (1997). Progress on binding CO₂ in mineral substrates. *Energy Conversion and Management*, 38, S259-S264. [https://doi.org/10.1016/S0196-8904\(96\)00279-8](https://doi.org/10.1016/S0196-8904(96)00279-8)
- Lelievre, P.G. & Oldenburg, D.W. (2009). A 3D total magnetization inversion applicable when significant, complicated remanence is present. *Geophysics*, 74,3, L21-L30. <https://library.seg.org/doi/10.1190/1.3103249>
- Lu, X. (2020). Characterization of ultramafic mine tailings reactivity for carbon capture and storage. M.Sc. Thesis, The University of British Columbia, 269 p.
- Maffione, M., Morris, A., Plümper, O., & van Hinsbergen, D. J. J. (2014). Magnetic properties of variably serpentinized peridotites and their implications for the evolution of oceanic core complexes. *Geochemistry, Geophysics, Geosystems*, 15. <https://doi.org/10.1002/2013GC004993>
- Milidragovic, D. (2019). Geology of the Cache Creek terrane north of Trembleur Lake. British Columbia Geological Survey Open File 2019-06, 1:50,000 scale.
- Milidragovic, D. & Grundy, R. (2019). Geochemistry and petrology of rocks in the Decar area, central British Columbia: petrologically constrained subdivision of the Cache Creek complex. *In: Geological Fieldwork 2018*, British Columbia Ministry of Energy, Mines and Petroleum Resources, British Columbia Geological Survey Paper 2019-01, 55–77.
- Milidragovic, D., Grundy, R., & Schiarizza, P. (2018). Geology of the Decar area north of Trembleur Lake, NTS 93K/14. *In: Geological Fieldwork 2018*, British Columbia Ministry of Energy, Mines and Petroleum Resources, British Columbia Geological Survey Paper 2018-01, 129–142.
- Miller, D. J., & Christensen, N. I. (1997). Seismic velocities of lower crustal and upper mantle rocks from the slow-spreading Mid-Atlantic Ridge, south of the Kane transform zone (MARK). *Proceedings from the Ocean Drilling Program Scientific Results*, 153, 437–454. <http://doi:10.2973/odp.proc.sr.153.043.1997>
- Mudd, G.M., & Jowitt, S.M. (2014). A detailed assessment of global nickel resource trends and endowments. *Economic Geology*, v.109, 1813–1841.
- Natural Resources Canada (2020): Canadian Airborne Geophysical Data Base, Airborne Geophysics Section, Geological Survey of Canada, Lands and Minerals Sector, Natural Resources Canada. <http://gdr.agg.nrcan.gc.ca/gdrdap/dap/search-eng.php>
- Nixon, G.T., Manor, M.J., Jackson-Brown, S., Scoates, J.S., & Ames, D.E. (2015). Magmatic Ni-Cu-PGE sulphide deposits at convergent margins. *In: Targeted Geoscience Initiative 4: Canadian nickel-copper-platinum group elements-chromium ore systems--fertility, pathfinders, new and revised models*, (eds.) D.E.Ames and M.G.Houle; Geological Survey of Canada, Open File 7856, p. 17–34.
- Nixon, G.T., Scheel, J.E., Friedman, R.M., Wall, C.J., Gabites, J., Miller, D., & Scoates, J.S. (2017). Geology and geochronology of the Turnagain ultramafic-mafic intrusion, British Columbia, British Columbia Ministry of Energy and Mines, British Columbia Geological Survey Geoscience Map 2017-1 (scale 1:10,000).
- Nixon, G.T., Scheel, J.E., Scoates, J.S., Friedman, R.M., Wall, C.J., Gabites, J., & Jackson-Brown, S. (2020). Syn-accretionary multistage assembly of an Early Jurassic Alaskan-type intrusion in the Canadian Cordillera: U-Pb and ⁴⁰Ar-³⁹Ar geochronology of the Turnagain ultramafic-mafic intrusive complex,

- Yukon-Tanana terrane. *Canadian Journal of Earth Sciences*, 57, 575–600.
- O’Hanley, D. S. (1996). Serpentinites, records of tectonic and petrological history. *In: Oxford Monographs on Geology and Geophysics* no. 34.
- Oufi, O., Cannat, M., & Horen, H. (2002). Magnetic properties of variably serpentinized abyssal peridotites. *Journal of Geophysical Research*, 107(5), EPM 3-1EPM 3-10. <https://doi:10.1029/2001JB000549>
- Power, I. M., Wilson, S. A., & Dipple, G. M. (2013). Serpentinite carbonation for CO₂ sequestration. *Elements*, 9, 115–121. <https://doi:10.2113/gselements.9.2.11>
- Power, I. M., Dipple, G. M., Bradshaw, P. M. D., & Harrison, A. L. (2020). Prospects for CO₂ mineralization and enhanced weathering of ultramafic mine tailings from the Baptiste nickel deposit in British Columbia, Canada. *International Journal of Greenhouse Gas Control*, 94, 102895. <https://doi.org/10.1016/j.ijggc.2019.102895>
- Seifritz, W. (1990). CO₂ disposal by means of silicates. *Nature*, 345, 486. <https://doi.org/10.1038/345486b0>
- Snæbjörnsdóttir, S.O., Sigfusson, B., Marieni, C., Goldberg, D., Gislasun, S.R., & Oelkers, E.H. (2020). Carbon dioxide storage through mineral carbonation. *Nature Reviews* 1:90–102.
- Steinthorsdottir, K., Cutts, J., Dipple, G., Milidragovic, D., & Jones, F. (2020). Origin and serpentinization of ultramafic rocks in dismembered ophiolite north of Trembleur Lake, central British Columbia. *In: Geological Fieldwork 2019, British Columbia Ministry of Energy, Mines and Petroleum Resources, British Columbia Geological Survey Paper 2020-01*, 49–58.
- Tauxe, L. (2010). *Essentials of Paleomagnetism*, 489 pp., University of California Press, Berkeley.
- Thom, J. M., Dipple, G. M., Power, I. M., & Harrison, A. L. (2013). Chrysotile dissolution rates: implications for carbon sequestration. *Applied Geochemistry*, 35, 244–254. <https://doi.org/10.1016/j.apgeochem.2013.04.016>
- Toft, P. B., Arkani-Hamed, J., & Haggerty, S. E. (1990). The effects of serpentinization on density and magnetic susceptibility: a petrophysical model. *Physics of the Earth and Planetary Interiors*, 65, 137–157. [https://doi.org/10.1016/0031-9201\(90\)90082-9](https://doi.org/10.1016/0031-9201(90)90082-9)
- Turvey, C.C., Wilson, S.A., Hamilton, J.L., Tait, A.W., McCutcheon, J., Beinlich, A., Fallon, S., Dipple, G., & Southam, G. (2018). Hydrotalcites and hydrated Mg-carbonates as carbon sinks in serpentinite mineral wastes from the Woodsreef chrysotile mine, New South Wales, Australia: Controls on carbonate mineralogy and efficiency of CO₂ air capture in mine tailings. *International Journal of Greenhouse Gas Control*, 79, 38–60.
- Vanderzee, S.S.S., Dipple, G.M., & Bradshaw, P.M.D. (2019). Targeting highly reactive labile magnesium in ultramafic tailings for greenhouse-gas offset and potential tailings stabilization at the Baptiste Deposit, central British Columbia (NTS 093K/13, 14). *Geoscience BC Summary of Activities 2018: Minerals and Mining, Geoscience BC, Report 2019-1*, 109–118.
- Wilson, S. A., Harrison, A. L., Dipple, G. M., Power, I. M., Barker, S. L. L., Mayer, K. U., Fallon, S. J., Raudsepp, M. & Southam, G. (2014). Offsetting of CO₂ emissions by air capture in mine tailings at the Mount Keith Nickel Mine, Western Australia: Rates, controls and prospects for carbon neutral mining. *International Journal of Greenhouse Gas Control*, 25, 121–140. <https://doi.org/10.1016/j.ijggc.2014.04.002>
- Zagorevski, A., Bedard, J.H., Bogatu, A., Coleman, M., Golding, M., & Joyce, N., (2017). Stikinia bedrock report of activities, British Columbia and Yukon: GEM2 Cordillera; Geological Survey of Canada Open File 8329, 13p. <https://doi.org/10.4095/306144>
- Zagorevski, A., van Staal, C.R., Bédard, J.H., Bogatu, A., Canil, D., Coleman, M., Golding, M., Joyce, N.J., Lawley, C., McGoldrick, S., Mihalyuk, M.G., Milidragovic, D., Parsons, A., & Schiarizza, P., In press. Overview of Cordilleran oceanic terranes and their significance for the tectonic evolution of the northern Cordillera. *Geologic Survey of Canada, Bulletin* 610.